

Interacting quark matter and $f(Q)$ gravity: A new paradigm in exploring the properties of quark stars

Debadri Bhattacharjee^{*1}, Koushik Ballav Goswami^{†2}, and Pradip Kumar Chattopadhyay^{‡3}

^{1,2,3}IUCAA Centre for Astronomy Research and Development (ICARD), Department of Physics, Cooch Behar Panchanan Barma University, Vivekananda Street, District: Cooch Behar, , Pin: 736101, West Bengal, India

January 22, 2025

Abstract

Perturbative Quantum Chromodynamics corrections and the colour superconductivity indicate that strongly interacting matter can manifest unique physical behaviours under extreme conditions. Motivated by this notion, we investigate the interior structure and properties of quark stars composed of interacting quark matter, which provides a comprehensive avenue to explore the strong interaction effects, within the framework of $f(Q)$ gravity. A unified equation of state is formulated to describe various phases of quark matter, including up-down quark matter ($2SC$), strange quark matter ($2SC+s$), and the Colour-Flavor Locked (CFL) phase. By employing a systematic reparametrisation and rescaling, the number of degrees of freedom in the equation of state is significantly reduced. Utilising the Buchdahl-I metric ansatz and a linear $f(Q)$ functional form, $f(Q) = \alpha_0 + \alpha_1 Q$, we derive the exact solutions of the Einstein field equations in presence of the unified interacting quark matter equation of state. For the $2SC$ phase, we examine the properties of quark stars composed of up-down quark matter. For the ($2SC+s$) and CFL phases, we incorporate the effects of a finite strange quark mass ($m_s \neq 0$). The Tolman-Oppenheimer-Volkoff equations are numerically solved to determine the maximum mass-radius relations for each phase. Our results indicate that the model satisfies key physical criteria, including causality, energy conditions, and stability requirements, ensuring the viability of the configurations. Furthermore, the predicted radii for certain compact star candidates align well with observational data. The study highlights that quark stars composed of interacting quark matter within the $f(Q)$ gravity framework provide a robust and physically consistent stellar model across all considered phases.

1 Introduction

Einstein's General Theory of Relativity (GR) has revolutionised our understanding of gravitational phenomena, from the solar system to cosmological scales [1]. Verified experimentally by Arthur Eddington in 1919, GR remains the most successful framework for explaining gravitational interactions. Its predictions have transformed ultra-dense compact objects, such as black holes (BH), neutron stars (NS), and white dwarfs (WD), from theoretical concepts into observable entities, particularly after the 1967 discovery of pulsars.

Recent advances in observational capabilities have greatly enhanced our understanding of high-energy phenomena at smaller cosmic scales, fostering significant interest in the behaviour of matter under the extreme densities and temperatures found in NS. Experimental replication of these conditions remains infeasible, making the equation of state (EoS) for dense matter heavily reliant on theoretical models [2, 3]. Considerable efforts have been directed toward addressing this challenge, particularly by exploring the fundamental composition of compact stars. Proposed forms of exotic matter include Bose-Einstein condensates, quark-gluon plasma, and high-temperature superconductors. For NS and quark stars, an accurate EoS for strongly interacting matter at high densities and low temperatures is vital, theoretically derivable from Quantum Chromodynamics (QCD). However, the non-perturbative nature of QCD at finite baryon densities and the lattice QCD "sign problem" complicate first-principles solutions [4]. At lower densities, nuclear interactions dominate and are modeled using relativistic or non-relativistic effective theories [5]. However, in the ultra-dense stellar core, densities surpass nuclear saturation, necessitating descriptions in terms of deconfined quarks. Due to the absence of more realistic models, this high-density regime often relies on simplified models like the MIT bag model [6], which incorporates a bag constant to encapsulate interaction effects. Itoh [7] first introduced the idea that NS interior may have sufficient housing conditions of

*debadriwork@gmail.com

†koushik.kbg@gmail.com

‡pkc_76@rediffmail.com

quark matter cores. Pioneering work by Madsen [8] established the significance of strange quarks for stability in compact stars, leading to the concept of Strange Stars (SS) or Strange Quark Stars (SQS) [8, 9, 10, 11], where Strange Quark Matter (SQM) is hypothesised as the QCD ground state [12].

However, the recent monumental work of Holdom et al. [13] demonstrated that if the flavour dependent feedback of gaseous quark assembly on QCD vacuum is considered, then, the bulk energy per baryon of quark matter composed of only u and d quarks (udQM) reduces in comparison to SQM. Hence, udQM can be relatively more stable compared SQM. Moreover, considering the finite size effects, the udQM can be termed the ground state of baryonic matter for sufficiently large baryon number density [13]. Interestingly, Zhang [14] has studied the udQM via gravitational waves and proposed a new interpretation for the binary merger event GW170817 where he showed that u and d quark stars (udQS) may be one of the components of the detected binary system, at least. Based on this fundamental principle, a number of phenomenological and experimental models have been postulated [14, 15, 16, 17, 18, 19]. Now, in the pursuit of a more realistic EoS, the strong interaction among the fundamental building blocks of matter must be taken into consideration. According to QCD, this fundamental interaction is largely influenced by the interactions among quarks and gluons. Consequently, QCD provides a comprehensive theoretical framework for understanding the behaviour of matter under extreme conditions, such as those found in the early universe or within SQS. In this context, the Interacting Quark Matter (IQM) has emerged as a prime candidate in describing the interior of SQS considering the impact of strong interaction and the vicinity of hyperdense compact cores. In light of the recent LIGO-VIRGO observations, many studies have shed light on the properties of SQS [20, 21, 23, 22, 24] and udQS [25, 26, 27] involving the presence of IQM. IQM accounts for the interquark effects arising from perturbative quantum chromodynamics (pQCD) and incorporates aspects of colour superconductivity. Now, the corrections due to pQCD are induced through the gluon mediated interactions [6, 28, 29]. Further, in the quark matter, the condensation of spin-0 Cooper pair, which are antisymmetric in the flavour space, gives rise to the colour superconductivity [30, 31, 32]. This can lead to the formation of two-flavour colour superconductivity, where u and d quarks form pairing interactions, or to a colour-flavour-locked (CFL) phase, where u , d and s quarks pair with one another in an antisymmetric configuration. The pairing of u and d is termed $2SC$ phase and if s quarks are introduced into the group, it is termed $2SC + s$ phase. Existing models of non-interacting SQM and udQM, with their current bag constant values, are inadequate to explain the unusually high mass of the observed lighter companion object of GW190814 [33]. This discrepancy has prompted interest in investigating whether strongly interacting quark stars (IQSs), composed of IQM, could fulfil these mass constraints and offer a viable model for the lighter companion's characteristics. Using this notion of IQM in IQS, researchers have investigated the possible formation of compact stars in different aspects of stellar modeling [34, 35, 36].

In this manuscript, we explore the possibility of IQS in the framework of $f(Q)$ gravity. Shortly after GR was introduced, Weyl [37] made the first modifications by incorporating higher-order invariants into the Einstein-Hilbert action, aiming to unify electromagnetism and gravitation. Over time, two primary geometrical modifications to GR emerged: extensions based on curvature-such as $f(R)$, $f(T)$, $f(R, T)$ theories-and extensions based on torsion and non-metricity, like $f(Q)$ gravity. Theories based on torsion and non-metricity [38], equivalent to GR, include the Teleparallel Equivalent of General Relativity (TEGR) [39, 40] and the Symmetric Teleparallel Equivalent of General Relativity (STEGR) [41]. In TEGR, gravity in flat spacetime with torsion is formulated using tetrads and spin connections as key variables. By constraining curvature and non-metricity tensors to zero, the Weitzenböck connection can be adopted, leaving tetrads as fundamental entities, and making this choice a gauge selection that does not alter the physical interpretation of the theory. In STEGR, however, gravity is characterised by non-metricity rather than curvature or torsion, with the 'coincidence gauge' setting the metric tensor as the primary variable.

An extension of STEGR, $f(Q)$ gravity, parallels $f(R)$ theory and has been widely applied [42, 43]. Hohmann et al. [44] studied gravitational wave polarization and propagation in Minkowski space within $f(Q)$ gravity, while Soudi et al. [45] found that gravitational wave polarization significantly impacts strong-field gravity. $f(Q)$ theory has been applied to late-time cosmic acceleration [46], black holes [47, 48], bouncing cosmologies [49], and observational constraints [50, 51]. Comprehensive reviews are available in several works [52, 53, 54, 55, 56, 57]. Recently, the $f(Q)$ theory has gained considerable attention in astrophysical research, offering new perspectives on compact stellar structures. Adeel et al. [58] presented a comprehensive approach to study the physical properties of compact stars in $f(Q)$ gravity. Maurya et al. [59] applied gravitational decoupling within $f(Q)$ gravity to explore mass and radius constraints for the lighter component of GW190814 and other self-bound strange stars. Errehymy et al. [60] proposed a singularity-free charged strange star model within $f(Q)$ gravity, while Lohakare et al. [61] analysed the impact of gravitational decoupling on the maximum mass and stability of strange stars under linear $f(Q)$ action. Additional studies have also incorporated $f(Q)$ theory in analysing stable stellar configurations [62, 63, 64, 65].

For a more accurate physical model, it is crucial to treat the interior fluid of dense compact objects as anisotropic. Ruderman [66] and Canuto [67] emphasised that anisotropic pressures may arise in compact stars at densities exceeding nuclear levels, with type 3A superfluidity potentially influencing the core dynamics [68]. Quantum mechanically, this superfluidity results from Cooper pair formation at low temperatures, leading to collective behaviors akin to He-3 superfluids [69]. Anisotropy may also originate from fermionic fields, electromagnetic interactions, pion condensation, or viscosity effects [70, 71, 72]. Bowers and Liang [73] introduced pressure anisotropy to analyse compactness and mass-radius

relations, while Heintzmann and Hillebrandt [74] showed that with sufficient anisotropy, mass and redshift limits remain unrestricted. Several studies [75, 76, 77, 78, 79, 80, 81, 82] have explored the impact of pressure anisotropy on the gross properties of relativistic stellar modeling.

Recent observations of massive pulsars and the quest for understanding extreme gravity regimes motivate us for exploring alternative theories of gravity. $f(Q)$ gravity, a modification of GR, offers a promising avenue to study compact objects like NS and SQS. Using an IQM EoS, which accounts for strong interactions between quarks at high densities, allows for a more realistic description of the stellar matter. By modeling stellar configurations in $f(Q)$ gravity with this EoS, we can investigate how modified gravity affects the properties of compact objects, potentially leading to new insights into the nature of gravity in extreme environments and the composition of dense matter. Recently, several studies have focused on maximum mass and radius relations of compact objects using the IQM EoS and anisotropy ansatz [34, 35, 36]. However, this is the first manuscript that presents a novel exact solution to the Einstein field equations (EFE) within the framework of $f(Q)$ gravity, uncovering intriguing aspects of the interior structure of quark stars.

The rest of the paper is organised in the following way: section 2 describes the properties of interacting quark matter and a parametrised unified quark matter EoS is established here. In section 3, we restrict the choice of parameter space through the evaluation of energy per baryon for different choices of colour superconductivity (Δ), strange quark mass (m_s) and bag constant (B_g). The mathematical fundamentals of $f(Q)$ gravity as expressed in section 4 and the exact solution of EFE in presence of IQM EoS and $f(Q)$ gravity is obtained in section 5. In GR, the constants of the model are evaluated by matching the interior solution and exterior vacuum Schwarzschild space-time at the stellar boundary. However, in presence of modified theories of gravity, this boundary conditions are subjected to modifications introduced by the concerned theories of gravity. Such modifications and the resulting boundary conditions are addressed in section 6. Section 7 demonstrates the determination of maximum mass and radius through the numerical solution of TOV equations for the $2SC$, $2SC + s$ and CFL phases. Additionally, we have provided predictions for the radii of few compact stars in this section. The physical validity of the proposed model, across the three phases, is established through the radial behaviour of key parameters, alongside verification of the causality condition and essential energy criteria, as discussed in section 8. Within the parameter space, the stability of the present model is assessed in section 9. Finally, we summarise the main findings of this study in section 10.

2 Properties of Interacting Quark Matter: Thermodynamics and Equation of State

Following the work of Alford and Rajagopal [83] and accounting for the pQCD corrections, we express the general form of the free energy (Ω) of superconducting quark matter as [84, 85]:

$$\Omega = -\frac{\xi_4}{4\pi^2}\mu^4 + \frac{\xi_4(1-a_4)}{4\pi^2}\mu^4 - \frac{\xi_{2a}\Delta^2 - \xi_{2b}m_s^2}{\pi^2}\mu^2 - \frac{\mu_e^4}{12\pi^2} + B_g, \quad (1)$$

where, μ and μ_e denote that average chemical potentials contributed by quarks and electrons respectively. In eq. (1), the first term is contributed by the distribution of unpaired free quark gas, the second term arises from the pQCD, specifically representing the effects of one-gluon exchange in gluon interactions up to the order of $\mathcal{O}(\alpha_s^2)$. Additionally, from a phenomenological perspective, the variation of a_4 from $a_4 = 1$ to very small values accounts for the higher order contributions [84, 85]. Notably, $a_4 = 1$ corresponds to a vanishing pQCD corrections. In the third term, the presence of m_s takes care of the finite value of strange quark mass and Δ represents the colour-superconductivity effects. In the last term, B_g is the bag constant which denotes the effective difference between the perturbative and non-perturbative vacuum energies and the size of B_g may depend on the choice of flavour [13]. According to the work of Zhang and Mann [26], we note that depending on the numerical values of the constant coefficients present in eq. (1), we obtain three different phases for the different types of quark matter present in the configuration, *viz.*,

$$(\xi_4, \xi_{2a}, \xi_{2b}) = \begin{cases} \left(\left[\left(\frac{1}{3} \right)^{\frac{4}{3}} + \left(\frac{2}{3} \right)^{\frac{4}{3}} \right]^{-3}, 1, 0 \right) & 2SC \text{ Phase} \\ \left(3, 1, \frac{3}{4} \right) & 2SC+s \text{ Phase} \\ \left(3, 3, \frac{3}{4} \right) & CFL \text{ Phase} \end{cases} \quad (2)$$

Now, the thermodynamic variables, such as energy density, pressure and quark number density can be extracted from the free energy (Ω) expressed in eq. (1) through the relations given below:

$$p = -\Omega, \quad n_q = -\frac{\partial\Omega}{\partial\mu}, \quad n_e = -\frac{\partial\Omega}{\partial\mu_e}, \quad \rho = \Omega + n_q\mu + n_e\mu_e, \quad (3)$$

Moreover, to narrow down the parameter space, we define a new parameter η as

$$\eta = \frac{\xi_{2a}\Delta^2 - \xi_{2b}m_s^2}{\sqrt{\xi_4 a_4}}. \quad (4)$$

Here, η characterises the strength of the strong interaction [26]. Using eq. (3), we obtain

$$n_q = \frac{\xi_4 a_4}{\pi^2} \mu^3 + \frac{\eta \sqrt{\xi_4 a_4}}{\pi^2} 2\mu, \quad n_e = \frac{\mu_e^3}{3\pi^2}, \quad (5)$$

and,

$$\rho = \frac{3\xi_4 a_4}{4\pi^2} \mu^4 + \frac{\mu_e^4}{4\pi^2} + \frac{\eta \sqrt{\xi_4 a_4}}{\pi^2} \mu^2 + B_g. \quad (6)$$

Using eq. (1) and eq. (6), we get the EoS in the form

$$p = \frac{1}{3}(\rho - 4B_g) + \frac{4\eta^2}{9\pi^2} \left(-1 + \sqrt{1 + 3\pi^2 \frac{(\rho - B_g)}{\eta^2}} \right). \quad (7)$$

However, in the present formalism, to obtain a tractable set of relativistic solutions of the Einstein field equation we parametrise the EoS in a linearised form as

$$p = \frac{1}{3}(\rho - 4B_{eff}), \quad (8)$$

where, $B_{eff} = B_g - \frac{3(\xi_{2a}\Delta^2 - \xi_{2b}m_s^2)}{4\pi^2} \mu^2 + \frac{\eta \sqrt{\xi_4 a_4}}{4\pi^2} \mu^2$. In the present context, the general linearised form of EoS provided above unifies the $2SC$, $2SC + s$ and CFL phases. Hence, we denote eq. (8) as the unified IQM EoS. Interestingly, for $\eta \rightarrow 0$ in eq. (7), we obtain the conventional non-interacting EoS for quark matter, whereas, for the other extreme end of limit, i.e, for $\eta \rightarrow \infty$, eq. (7) proceeds towards a special form as given below:

$$p = \rho - 2B_g. \quad (9)$$

From eq. (9), we note that, the inclusion of strong interaction reduces the surface mass density of quarks from $4B_g$, for non-interacting quark systems, to $2B_g$ in case of IQS. Moreover, the sound velocity for quark matter increases from $\frac{dp}{d\rho} = \frac{1}{3}$ up to 1.

3 Constraining the choice of Δ and m_s for different phases

One way to characterise the necessary constraints, on the permissible numerical values of colour superconductivity (Δ) and strange quark mass (m_s) for the three different phases, is through the evaluation of energy per baryon number (\mathcal{E}_B). The energy per baryon (\mathcal{E}_B) of the most stable nuclei, i.e., ${}^{56}\text{Fe}$ is 930.4 MeV . Hence, for the quark assembly in $2SC$, $2SC + s$, and, CFL phases, if the values of \mathcal{E}_B are less than 930.4 MeV , the configuration can be termed stable. In this section, we have studied the variation of \mathcal{E}_B with respect to Δ for different choices of m_s and a bag constant $B_g = 70 \text{ MeV}/f\text{m}^3$ and the results are graphically represented. Figure 1, represents the variation of energy per baryon (\mathcal{E}_B) with respect to

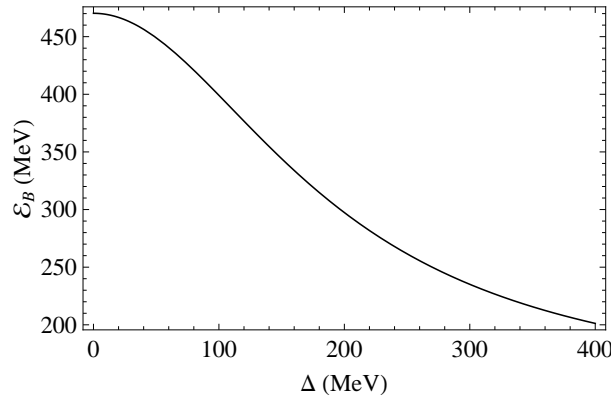


Figure 1: Energy per baryon, (\mathcal{E}_B) vs. colour superconductivity, (Δ) for $2SC$ phase

colour superconductivity (Δ) in $2SC$ phase. It is observed that the udQM actually possesses a lower energy per baryon number in comparison to SQM, which aids to the higher stability of udQM. Further, from figure 2, we note the influence of strange quark mass (m_s) on \mathcal{E}_B for $2SC + s$ and CFL phases respectively. Figure 2 demonstrates that for particular value of Δ , \mathcal{E}_B increases with increasing value of m_s . However, the numerical values of \mathcal{E}_B for the maximum value of m_s considered in this manuscript, i.e., $m_s = 100 \text{ MeV}$, remains well within the stable SQM range for $2SC + s$ and CFL phases respectively. Therefore, from figures 1 and 2, we note that the numerical choices for strange quark mass (m_s), bag constant $B_g = 70 \text{ MeV}/f\text{m}^3$ and a superconductivity parameter, $\Delta = 100 \text{ MeV}$, are suitable in the present formalism. Further, we note that for the above parametric choice of Δ and B_g , the maximum allowed value of strange quark mass (m_s) that ensures $\mathcal{E}_B < 930.4 \text{ MeV}$ are 262 MeV and 308 MeV for $2SC + s$ and CFL phases respectively.

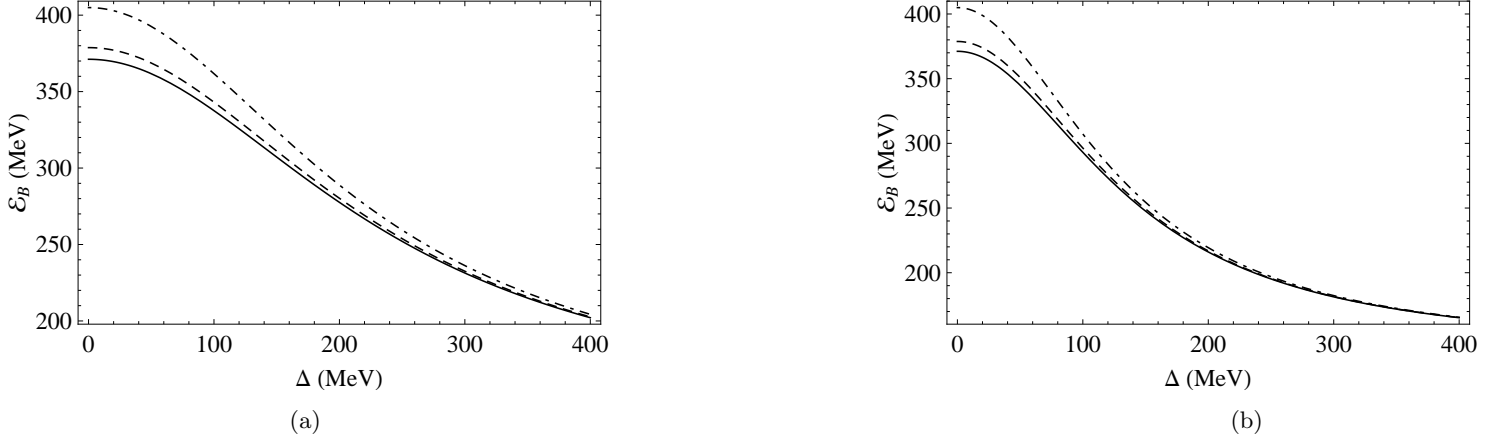


Figure 2: Energy per baryon, (\mathcal{E}_B) vs. colour superconductivity, (Δ) for (a) $2SC + s$ phase and (b) CFL phase. Here, the solid, dashed and dotdashed lines represent $m_s = 0, 50$ and 100 MeV respectively.

4 Fundamentals of $f(Q)$ gravity

In the framework of symmetric teleparallel $f(Q)$ gravity, the action integral is represented as follows:

$$\mathfrak{S} = \int \sqrt{-g} d^4x \left[\frac{1}{2} f(Q) + \lambda_i^{kij} R_{kij}^l + \tau_k^{ij} T_{ij}^k + \mathfrak{L}_m \right], \quad (10)$$

Here, g represents the determinant of the fundamental metric tensor g_{ij} , i.e., $g = |g_{ij}|$. The function $f(Q)$ relates to non-metricity Q . The terms λ_i^{kij} and τ_k^{ij} are Lagrangian multipliers, R_{kij}^l denotes the Riemann tensor, and T_{ij}^k is the torsion tensor. The Lagrangian densities for matter is described by \mathfrak{L}_m . In terms of the affine connection (Γ_{ij}^k), the non-metricity is expressed as:

$$Q_{kij} = \nabla_k g_{ij} = \delta_k g_{ij} - \Gamma_{ij}^l g_{lj} - \Gamma_{ik}^l g_{jl}. \quad (11)$$

Here, ∇_k denotes the covariant derivative. Additionally, the affine connection can be decomposed into three components as follows:

$$\Gamma_{ij}^k = \epsilon_{ij}^k + K_{ij}^k + L_{ij}^k. \quad (12)$$

In eq. (12),

- The Levi-Civita connection, denoted as ϵ_{ij}^k , is defined in terms of the fundamental metric tensor g_{ij} as follows:

$$\epsilon_{ij}^k = \frac{1}{2} g^{kl} \left(\partial_i g_{lj} + \partial_j g_{il} - \partial_l g_{ij} \right). \quad (13)$$

- The contorsion, described by K_{ij}^k , is expressed as:

$$K_{ij}^k = \frac{1}{2} T_{ij}^k + T_{(i k j)}. \quad (14)$$

In the context of STEGR, the contorsion K_{ij}^k corresponds to the antisymmetric component of the affine connection, which is mathematically expressed as: $T_{ij}^k = 2\Gamma_{[ij]}^k = \Gamma_{ij}^k - \Gamma_{ji}^k$.

- The term L_{ij}^k expresses the deformation and is written as:

$$L_{ij}^k = \frac{1}{2} Q_{ij}^k + Q_{(i k j)}. \quad (15)$$

The superpotential related to non-metricity is defined as

$$P^{kij} = -\frac{1}{4} Q^{kij} + \frac{1}{2} Q^{(ij)k} + \frac{1}{4} (Q^k - \tilde{Q}^k) g^{ij} - \frac{1}{4} \delta^{k(i} Q_{j)}, \quad (16)$$

where, Q^k and \tilde{Q}^k represent the independent traces of Q_{kij} and are written as:

$$Q_k \equiv Q_{ki}, \quad \tilde{Q}^k = Q_i^{ki}. \quad (17)$$

Hence, the non-metricity scalar can be formulated as:

$$Q = -g^{ij} \left(L_{ij}^k L_{ik}^l - L_{il}^l L_{ij}^k \right) = -Q_{kij} P^{kij}. \quad (18)$$

Now, we derive the gravitational field equations by varying the Einstein-Hilbert action, as expressed in eq. (10), with respect to the metric tensor g_{ij} , yielding the following expression:

$$\frac{2}{\sqrt{-g}} \nabla_k \left(\sqrt{-g} f_Q P_{ij}^k \right) + \frac{1}{2} g_{ij} f + f_Q \left(P_{ikl} Q_j^{kl} - 2Q_{kli} P_j^{kl} \right) = -T_{ij}, \quad (19)$$

where, $f_Q = \frac{\partial f}{\partial Q}$ and T_{ij} represents the energy-momentum tensor associated to the contribution of matter distribution. In a more general manner, we can describe the energy-momentum (T_{ij}) is the form:

$$T_{ij} = -\frac{2}{\sqrt{-g}} \frac{\delta(\sqrt{-g} \mathcal{L}_m)}{\delta g^{ij}}. \quad (20)$$

5 Exact solution of EFE in the framework of $f(Q)$ gravity with IQM EoS

To reiterate, this study explores a novel generalised approach to modeling quark stars within the framework of $f(Q)$ gravity. Now, the static spherically symmetric spacetime, a cornerstone assumption in gravitational theories, provides significant insights into diverse astrophysical phenomena. Accordingly, a static spherically symmetric spacetime has been adopted for the analysis in this work. In the static spherically symmetric curvature coordinate system, (t, r, θ, ϕ) , the line element is represented in the form:

$$ds^2 = -e^{2\nu(r)} dt^2 + e^{2\lambda(r)} dr^2 + r^2(d\theta^2 + \sin^2\theta d\phi^2). \quad (21)$$

Substituting eq. (21) in eq. (18), we obtain the following expression of the non-metricity as given below:

$$Q = -\frac{2e^{-2\lambda(r)}}{r} \left(2\nu'(r) + \frac{1}{r} \right), \quad (22)$$

Here, the prime indicates differentiation with respect to the radial coordinate r . Notably, Q depends on a mathematical framework where parallel transport within the Q -geometry involves neither rotations nor distortions. In essence, Q is constructed based on the vanishing coefficients of the affine connections. Further, the anisotropic perfect fluid distribution is defined as:

$$T_{ij} = (\rho + p_t) u_i u_j + p_t g_{ij} + (p_r - p_t) v_i v_j, \quad (23)$$

Here, u_i denotes the four-velocity of the anisotropic perfect fluid, while v_i represents the spacelike unit vector oriented along the radial direction. These quantities satisfy the conditions $u^i u_i = -1$ and $v^i v_i = 1$. In Eq. (23), ρ , p_r and p_t correspond to the energy density, radial pressure, and tangential pressure of the fluid, respectively. By combining the equation of motion from Eq.(19) with the anisotropic perfect fluid distribution described in Eq.(23), we derive a generalised set of non-zero components of the Einstein field equations in the following form:

$$\frac{f(Q)}{2} - f_Q \left[Q + \frac{1}{r^2} + \frac{2e^{-2\lambda}}{r} (\nu' + \lambda') \right] = 8\pi\rho, \quad (24)$$

$$-\frac{f(Q)}{2} + f_Q \left[Q + \frac{1}{r^2} \right] = 8\pi p_r, \quad (25)$$

$$-\frac{f(Q)}{2} + f_Q \left[\frac{Q}{2} - e^{-2\lambda} \left\{ \nu'' + 2 \left(\frac{\nu'}{2} + \frac{1}{2r} \right) (\nu' - \lambda') \right\} \right] = 8\pi p_t, \quad (26)$$

$$\frac{\cot\theta}{2} Q' f_{QQ} = 0, \quad (27)$$

where the prime ($'$) denotes differentiation with respect to r . Utilising eq. (27), we obtain the form of the linear $f(Q)$ action, which is expressed as:

$$f(Q) = \alpha_0 + \alpha_1 Q, \quad (28)$$

Here, α_0 carries the dimension of $K m^{-2}$, while α_1 is a dimensionless parameter. Utilising eqs. (24), (25), (26), (27), and (28), the field equations within the framework of the modified $f(Q)$ gravity are simplified to an exact set of expressions as follows:

$$\frac{1}{2r^2} \left[r^2 \alpha_0 - 2\alpha_1 e^{-2\lambda} (2r\lambda' - 1) - 2\alpha_1 \right] = 8\pi\rho, \quad (29)$$

$$\frac{1}{2r^2} \left[-r^2 \alpha_0 - 2\alpha_1 e^{-2\lambda} (2r\nu' + 1) + 2\alpha_1 \right] = 8\pi p_r, \quad (30)$$

$$\frac{e^{-2\lambda}}{2r} \left[-r\alpha_0 e^{2\lambda} - 2r\alpha_1 \nu'' - 2\alpha_1 (r\nu' + 1) (\nu' - \lambda') \right] = 8\pi p_t. \quad (31)$$

To derive the exact set of solutions within this formalism, we apply the Buchdahl-I ansatz [86], which encompasses nearly all solutions of the static EFE coupled with a perfect fluid distribution. This ansatz is expressed as follows:

$$e^{2\lambda} = \frac{2(1 + \chi r^2)}{2 - \chi r^2}, \quad (32)$$

Substituting the metric ansatz, as given in eq. (32), in eq. (29), we obtain the analytical expression of the energy density (ρ) as:

$$\rho = \frac{\alpha_0 + 2\alpha_0\chi r^2 - 9\alpha_1\chi + \alpha_0\chi^2 r^4 - 3\alpha_1\chi^2 r^2}{16\pi(1 + \chi r^2)^2}. \quad (33)$$

Now, employing eq. (33) in the generalised IQM EoS, expressed in eq. (8), we obtain the expression for radial pressure p_r in the form:

$$p_r = \frac{1}{3} \left(\frac{\alpha_0 + 2\alpha_0\chi r^2 - 9\alpha_1\chi + \alpha_0\chi^2 r^4 - 3\alpha_1\chi^2 r^2}{16\pi(1 + \chi r^2)^2} - 4B_g \right). \quad (34)$$

Substituting eq. (34) in eq. (30), we obtain the metric potential of the $g_{tt}(= e^{2\nu})$ component in the following form:

$$\nu = \frac{\left((6\alpha_0 - 7\alpha_1\chi - 96\pi B_g) \log[\chi r^2 - 2] + \chi(2\alpha_0 r^2 - 32\pi B_g r^2 + 6\alpha_1 + \alpha_1 \log[1 + \chi r^2]) \right)}{6\alpha_1\chi}. \quad (35)$$

Now, employing eqs. (32) and (35) in eq. (31), we get the tangential pressure (p_t) in the form:

$$p_t = \frac{1}{144\pi\alpha_1(\chi r^2 - 2)(1 + \chi r^2)^3} \left(4\alpha_0^2 + \chi^4 r^{10} + 6\alpha_1(9\alpha_1\chi - \alpha_0) + f_1 + f_2 + f_3 + f_4 + f_5 + f_6 \right), \quad (36)$$

where, $f_1 = 1024\pi^2 B_g^2 r^2 (1 + \chi r^2)^4$,

$$f_2 = \alpha_0 \chi^3 r^8 (16\alpha_0 - 21\alpha_1\chi),$$

$$f_3 = 3r^6 \chi^2 (8\alpha_0^2 - 33\alpha_0\alpha_1\chi + 12\alpha_1^2 \chi^2),$$

$$f_4 = r^2 (4\alpha_0^2 - 69\alpha_0\alpha_1\chi + 117\alpha_1^2 \chi^2),$$

$$f_5 = r^4 \chi (16\alpha_0^2 - 141\alpha_0\alpha_1\chi + 171\alpha_1^2 \chi^2),$$

$$f_6 = -32\pi B_g (1 + \chi r^2)^2 (-12\alpha_1 + 4r^6 \alpha_0 \chi^2 + r^2 (4\alpha_0 - 33\alpha_1\chi) + 2r^4 \chi (4\alpha_0 - 3\alpha_1\chi)).$$

The pressure anisotropy, i.e., the difference between radial and tangential pressures is expressed as:

$$\Delta_a = p_t - p_r. \quad (37)$$

The total active gravitational mass enclosed within a spherical volume of radius R is given by,

$$m(r) = 4\pi \int_0^R \rho r^2 dr. \quad (38)$$

6 Boundary conditions

To proceed, let us impose the boundary condition necessary for determining the constants and physical parameters to analyse the properties of the compact star. This involves ensuring a smooth matching of the interior spacetime to an appropriate exterior vacuum solution at the surface of vanishing pressure (i.e., at $r = R$). Specifically, for the functional form of $f(Q) = \alpha_0 + \alpha_1 Q$, we follow the approach outlined by Wang et al.[87]. For the off-diagonal component given in eq. (23), the solutions in the $f(Q)$ gravity framework are constrained to two specific cases:

$$f_{QQ} = 0, \Rightarrow f(Q) = \alpha_0 + \alpha_1 Q, \quad (39)$$

$$Q' = 0, \Rightarrow Q = Q_0, \quad (40)$$

where α_0 , α_1 , and Q_0 are constants. It is important to observe that these results parallel those obtained in $f(T)$ gravity as discussed by Böhmer et al. [88], where the constraints $f_{TT} = 0$ or $T' = T_0$ were employed for static, spherically symmetric configurations under a diagonal tetrad formalism. Moreover, if the cosmological constant is defined as $\frac{\alpha_0}{\alpha_1}$, the first solution in eq. (39) effectively reduces to GR, as it aligns with symmetric teleparallel general relativity.

In the case of a vacuum, the physical quantities ρ , p_r , and p_t all vanish. Consequently, the equations of motion, eqs. (22), (24), (25), (26), in light of eq. (39), reduce to the following forms:

$$\lambda'(r) + \nu'(r) = 0, \quad (41)$$

$$Q = \frac{\alpha_0}{\alpha_1} - \frac{2}{r^2}. \quad (42)$$

From eq. (41), we obtain:

$$\nu(r) = -\lambda(r) + \lambda_0, \quad (43)$$

where λ_0 is an integration constant that can be absorbed into the solution by rescaling the time coordinate from t to $e^{-\lambda_0}t$. As a result, the components g_{rr} and g_{tt} become reciprocal to one another, as noted by Wang et al. [87]. Therefore, eq. (43) simplifies to:

$$\nu(r) = -\lambda(r). \quad (44)$$

Using eqs. (21), (41) and (42), the expression for the exterior g_{rr} component is derived as:

$$e^{2\lambda} = \left(1 - \frac{c_1}{r} - \frac{\alpha_0}{6\alpha_1}r^2\right)^{-1}, \quad (45)$$

where c_1 is an integration constant, and its sign is chosen for convenience. Similarly, using eqs. (44) and 45, the g_{tt} component is obtained as:

$$e^{2\nu} = \left(1 - \frac{c_1}{r} - \frac{\alpha_0}{6\alpha_1}r^2\right). \quad (46)$$

Thus, the line element for the spherically symmetric vacuum exterior spacetime, within the framework of $f(Q)$ theory of gravity, describing a compact stellar configuration can be expressed as:

$$ds^2 = \left(1 - \frac{c_1}{r} - \frac{\alpha_0}{6\alpha_1}r^2\right) dt^2 + \left(1 - \frac{c_1}{r} - \frac{\alpha_0}{6\alpha_1}r^2\right)^{-1} dr^2 + r^2(d\theta^2 + \sin^2\theta d\phi^2). \quad (47)$$

Analysing the metric in Equation (47) reveals three key features: (i) when $c_1 = 2M$, and (ii) when the cosmological constant $\Lambda = \frac{\alpha_0}{\alpha_1}$, the metric reduces to the Schwarzschild-(anti) de Sitter solution:

$$ds^2 = \left(1 - \frac{2M}{r} - \frac{1}{3}\Lambda r^2\right) dt^2 + \left(1 - \frac{2M}{r} - \frac{1}{3}\Lambda r^2\right)^{-1} dr^2 + r^2(d\theta^2 + \sin^2\theta d\phi^2), \quad (48)$$

where M represents the total mass of the stellar configuration with radius R . In the absence of the cosmological constant, the metric reduces further to the Schwarzschild solution [89]:

$$ds^2 = -\left(1 - \frac{2M}{r}\right) dt^2 + \left(1 - \frac{2M}{r}\right)^{-1} dr^2 + r^2(d\theta^2 + \sin^2\theta d\phi^2). \quad (49)$$

Therefore, the observed correspondence between eqs. (47) and (48) strongly suggests that such solutions are attainable only under linear form of $f(Q)$ gravity. This linearity condition effectively reduces the theory to a form equivalent GR. Again, following Wang et al. [87], we note that, when a non-trivial functional form of $f(Q)$ is considered, the exact Schwarzschild solutions are not possible.

In modified theories of gravity, the equations of motion prescribed by GR are altered, necessitating corresponding modifications to the boundary conditions typically applied to stellar systems in GR [90]. Within the 4-dimensional spacetime manifold (Σ), there are two distinct regions: the interior and exterior spacetimes. These regions are separated by a 3-dimensional hypersurface (Ξ), which is characterised by the induced metric h_{ij} in the coordinate system X^i , with indices excluding the direction orthogonal to Ξ . The projection tensors and the normal vector are expressed as $e_i^a = \frac{\partial x^a}{\partial X^i}$ and $n_a = \epsilon \delta_a \ell$, where ℓ represents the affine connection in the direction perpendicular to Ξ , and ϵ takes values of -1 , 0 or 1 for the respective timelike, null, and spacelike geodesics. Given this setup, we have $n^a e_i^a = 0$. The induced metric h_{ij} and the extrinsic curvature tensor K_{ij} at the hypersurface are then written as:

$$h_{ij} = e_i^a e_j^b g_{ab}, \quad K_{ij} = e_i^a e_j^b \nabla_a n_b. \quad (50)$$

In the distribution formalism introduced by Rosa et al. [91], the condition $[h_{ij} = 0]$ is imposed, ensuring the continuity of the induced metric at the hypersurface Ξ . To determine the constants in the metric potentials, it is essential to also

require the continuity of the extrinsic curvature tensor at the junction. In the absence of a thin shell, this continuity condition is expressed as $[K_{ij} = 0]$ [91]. To calculate the extrinsic curvature, we start by considering the vacuum exterior solution obtained in eq. (49). Notably, in the parametric space of spherically symmetric spacetime, K_{ij}^{\pm} consists of only two components: K_{00} and $K_{\theta\theta} = K_{\phi\phi}\sin^2\theta$, where (+) and (-) signs correspond to the exterior and interior spacetimes, respectively. Using Eq. (50), we calculate the extrinsic curvature tensors for the interior and exterior spacetimes. By matching these tensors at the stellar boundary ($r = R$), we derive the following result:

$$\chi = -\frac{4M}{R^2(4M - 3R)}. \quad (51)$$

Moreover, another essential condition is that the radial pressure vanishes at the surface of the star, i.e.,

$$p_r(r = R) = 0. \quad (52)$$

Eq. (52) is employed to derive the expression for stellar radius in the present model. However, to simplify the presentation and avoid complex mathematical expressions, we have instead tabulated the numerical values of the radii for the *2SC*, *2SC + s* and *CFL* phases for the compact star under consideration.

7 Determination of mass-radius relation from TOV equation

To obtain the maximum mass and the associated radius in presence of IQM EoS expressed in eq. (8), we have numerically solved the Tolman-Oppenheimer-Volkoff equations [92, 93], considering bag constant, $B_g = 70 \text{ MeV}/f\text{m}^3$, colour superconductivity, $\Delta = 100 \text{ MeV}$ and different choices of strange quark mass, *viz.*, $m_s = 0, 50$ and 100 MeV for *2SC*, *2SC + s* and *CFL* phases respectively. We illustrate the concerned results below. Figure 3 demonstrates the maximum

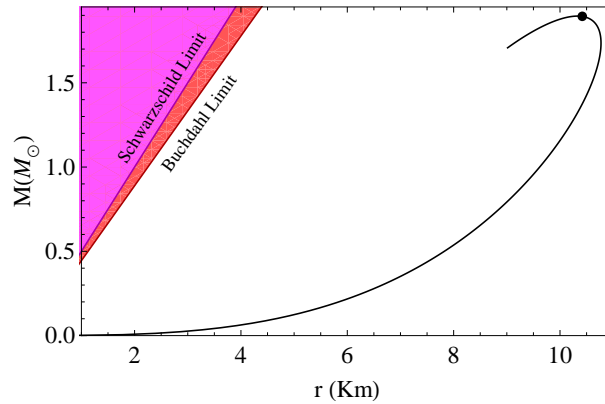


Figure 3: Mass-radius diagram for *2SC* phase.

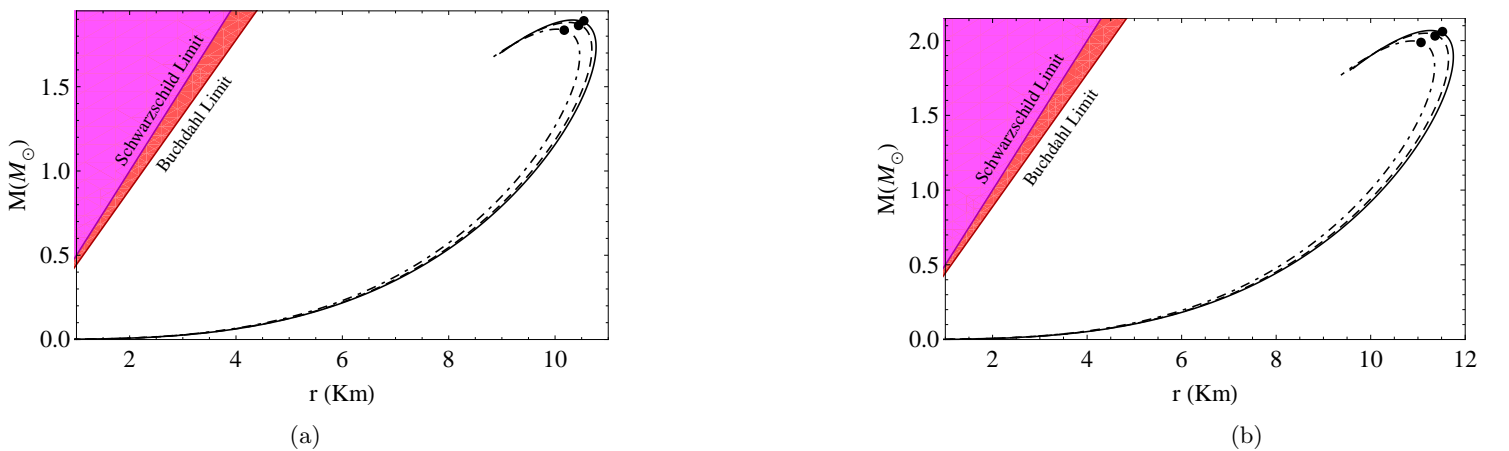


Figure 4: Mass-radius diagram for (a) *2SC + s* phase and (b) *CFL* phase. Here, the solid, dashed and dot-dashed lines represent $m_s = 0, 50$ and 100 MeV respectively.

mass-radius plot for uQM matter in *2SC* phase. Whereas, from figure 4, we note that with increasing strange quark mass

(m_s), both the maximum mass and radius decrease for the $2SC + s$ and CFL phases respectively. This can be explained by the fact that a higher m_s leads to an increase in the associated Fermi energy, as the Fermi energy of degenerate fermions depends on both the mass and Fermi momentum of the strange quark. Consequently, the EoS becomes softer thereby decreasing the maximum mass further. Additionally, a higher strange quark mass lowers the quark number density for a given pressure, as more massive quarks require greater energy. This results in fewer quarks being accommodated in a given volume at fixed pressure, causing a rapid rise in energy density at higher baryon number densities. The increased energy density accelerates gravitational collapse, leading to a reduction in both the maximum mass and the corresponding radius. Thus, as m_s increases, the EoS softens, causing a decrease in the maximum mass, as illustrated in Fig. (4). The maximum mass and the corresponding radii are tabulated in table 1. Following figures 3 and 4 and table 1, a comparison

Phase	Strange quark mass (m_s)	M_{max} (M_\odot)	R (Km)
$2SC$	–	1.89	10.34
$2SC + s$	0	1.89	10.34
	50	1.88	10.25
	100	1.84	10.04
CFL	0	2.07	11.27
	50	2.05	11.17
	100	1.99	10.89

Table 1: Tabulation of maximum mass and the associated radius for $2SC$, $2SC + s$ and CFL phases respectively.

of the three phases on the basis of mass-radius relation reveals that CFL phase actually accommodates a more massive stellar structure relative to the other phases [94]. Further, we have predicted the radii of some known compact stars in table 2. Additionally, tables 3 and 4 describe the central parameters such as central density (ρ_0), surface density (ρ_s) and central pressure (p_0) for $2SC$, $2SC + s$ and CFL phases respectively.

Compact objects	Observed mass (M_\odot)	Observed radius (Km)	Radius prediction			
			$2SC$ (Km)	m_s (MeV)	$2SC + s$ (Km)	CFL (Km)
EXO 1745-248 [95]	1.4	11	10.52	50	10.46	11.18
4U 1820-30 [96]	$1.58^{+0.06}_{-0.06}$	$9.1^{+0.4}_{-0.4}$	10.68	250	9.10	9.77
LMC X-4 [97]	$1.04^{+0.09}_{-0.09}$	$8.301^{+0.2}_{-0.2}$	9.72	250	8.64	9.05
HER X-1 [98]	$0.85^{+0.15}_{-0.15}$	$8.1^{+0.41}_{-0.41}$	9.17	200	8.51	8.93
PSR J1903+0327 [99]	$1.667^{+0.021}_{-0.021}$	$9.438^{+0.03}_{-0.03}$	10.75	200	9.57	10.36

Table 2: Radius prediction of some known compact objects from TOV mass-radius relation in $2SC$, $2SC + s$ and CFL phases respectively.

Compact objects	$2SC$ phase		
	$\rho_0 \times 10^{15}$ (gm/cm^3)	$\rho_s \times 10^{15}$ (gm/cm^3)	$p_0 \times 10^{34}$ (dyn/cm^2)
EXO 1745-248	0.46	0.28	0.10
4U 1820-30	0.52	0.30	1.81
LMC X-4	0.47	0.32	0.48
HER X-1	0.46	0.32	0.09
PSR J1903+0327	0.55	0.30	2.68

Table 3: Tabulation of central parameters of few known compact objects for $2SC$ phase.

Compact objects	2SC phase			CFL phase		
	$\rho_0 \times 10^{15}$ (gm/cm^3)	$\rho_s \times 10^{15}$ (gm/cm^3)	$p_0 \times 10^{34}$ (dyn/cm^2)	$\rho_0 \times 10^{15}$ (gm/cm^3)	$\rho_s \times 10^{15}$ (gm/cm^3)	$p_0 \times 10^{34}$ (dyn/cm^2)
EXO 1745-248	0.47	0.28	0.16	0.40	0.25	0.10
4U 1820-30	0.91	0.46	8.23	0.71	0.38	4.45
LMC X-4	0.63	0.41	0.04	0.56	0.37	0.09
HER X-1	0.58	0.40	0.23	0.50	0.36	0.14
PSR J1903+0327	0.82	0.42	7.60	0.62	0.34	3.82

Table 4: Tabulation of central parameters of few known compact objects for 2SC + s and CFL phases.

8 Physical attributes of the proposed model

For a stellar model to be considered physically viable, it is essential that the associated physical parameters derived from the model are realistic and consistent with observable phenomena. To qualify as a compact star, the model must satisfy the fundamental conditions of regularity and physical plausibility that are inherent to relativistic stellar structures. In this pursuit, we have considered the Low-Mass X-ray Binary (LMXB) 4U 1608-52, having a mass of $1.74 M_\odot$ [100], to study the physical viability of the present model under the combined influence of interacting quark system and $f(Q)$ formalism. Moreover, following the work of Maurya et al. [101], we have considered $\alpha_0 = 10^{-46} Km^{-2}$ and $\alpha_1 = -0.6$ as arbitrary choices. Now, to start with, we have used eq. (52) to estimate the radii of LMXB 4U 1608-52 for different values of m_s across the three phases, within the framework of $f(Q)$ theory of gravity and the results are tabulated in table 5. From table 5, it is evident that as m_s increases the radius decreases which points towards a softer EoS. Notably, in describing the physical characteristics of the present model, we have used the radii from table 5 for the three phases.

Phases	Strange quark mass (m_s)	Predicted radius (Km)
2SC	–	9.33
2SC + s	0	9.33
	50	9.28
	100	9.13
CFL	0	9.95
	50	9.89
	100	9.70

Table 5: Radius prediction for 4U 1608-52 from model.

8.1 Radial variation of thermodynamic parameters

For a realistic stellar configuration, the behaviour of the inherent thermodynamic attributes, i.e., energy density (ρ), radial (p_r) and tangential (p_t) components of pressure and pressure anisotropy (Δ_a), must maintain certain viability conditions which are discussed below:

- **Energy Density:** Figures 5 and 6 show the diagram of ρ vs. r for the three phases respectively. The energy density (ρ) of udQM phase is shown in figure 5. From figures 6a and 6b, we note that as m_s increases, the energy density (ρ) of the quarks, in 2SC + s and CFL phases, increases. The energy density reaches a peak value at the core and thereafter diminishes towards the stellar boundary which describes a physically viable stellar model.

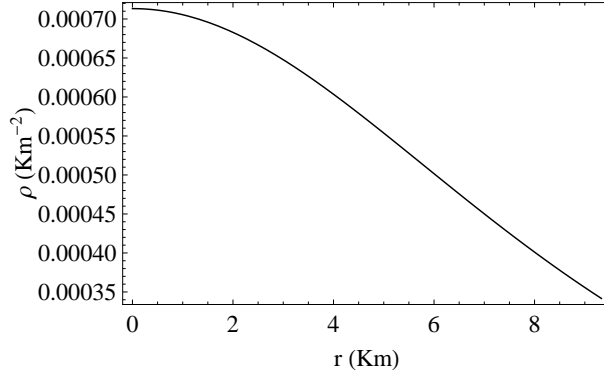


Figure 5: Radial variation of energy density (ρ) for $2SC$ phase.

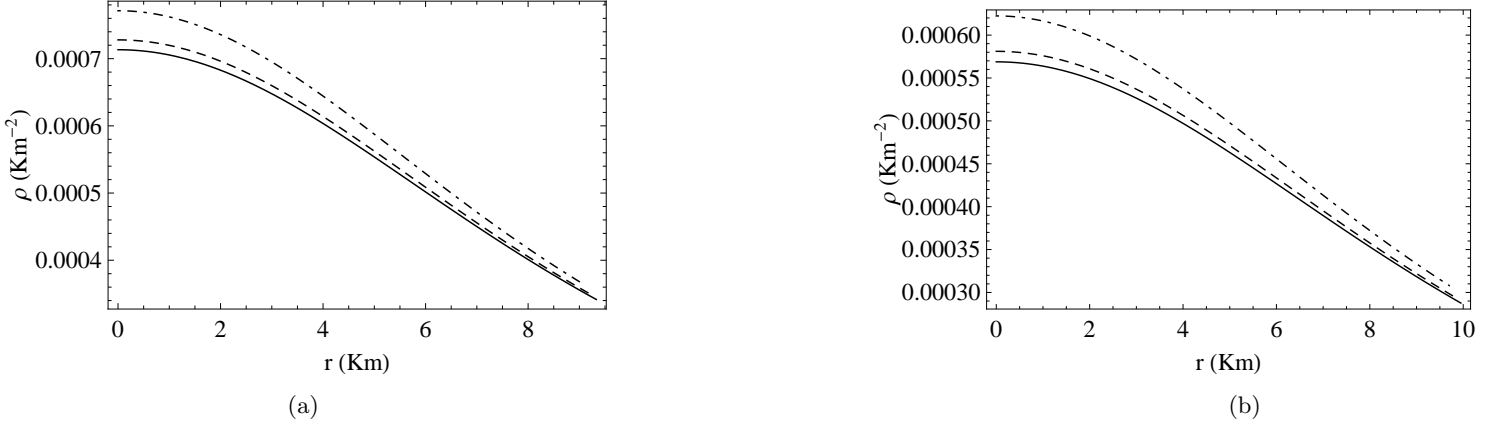


Figure 6: Radial variation of energy density (ρ) for (a) $2SC + s$ phase and (b) CFL phase. Here, the solid, dashed and dotdashed lines represent $m_s = 0, 50$ and 100 MeV respectively.

- Radial pressure:** The radial pressure counterbalances the inward gravitational force which prevents the collapse of compact stars under their own weight. Moreover, for a physically realistic model, the variation of the radial pressure (p_r) with respect to radial parameter (r) must be monotonically decreasing from centre to the stellar surface which is depicted in figures 7 and 8. Figures 7, 8a and 8b illustrate the radial pressure profiles for the $2SC$, $2SC + s$ and CFL phases respectively. Evidently, from figure 8, with increasing strange quark mass (m_s), the radial pressure increases. However, due to the decreasing energy density towards the boundary, the magnitude of radial pressure diminishes.

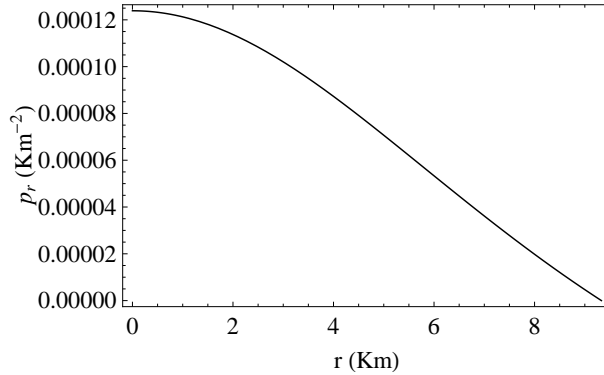


Figure 7: Radial variation of radial pressure (p_r) for $2SC$ phase.

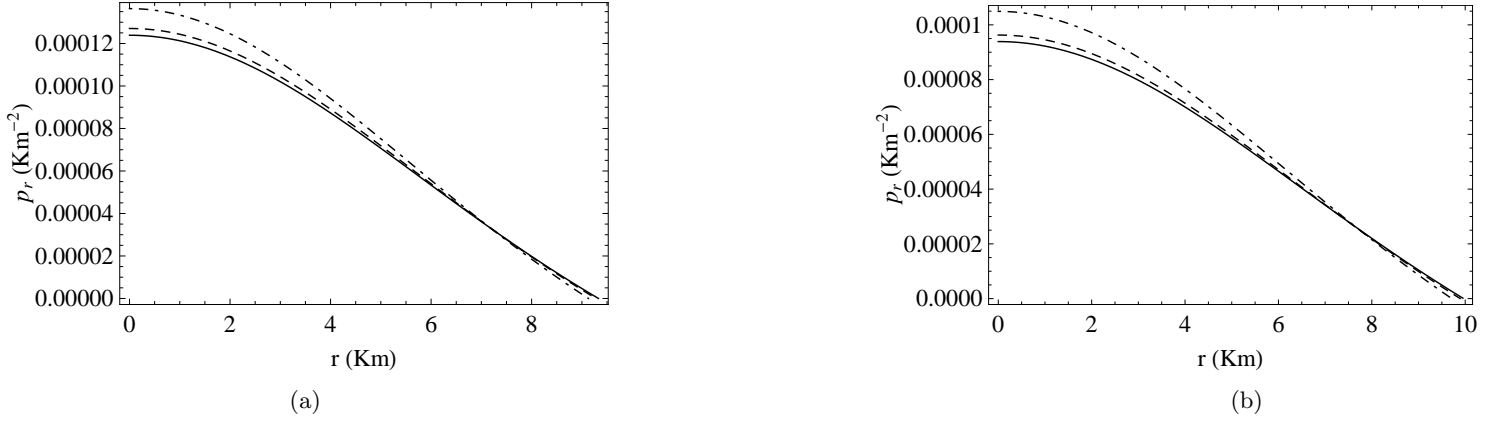


Figure 8: Radial variation of radial pressure (p_r) for (a) $2SC + s$ phase and (b) CFL phase. Here, the solid, dashed and dotdashed lines represent $m_s = 0, 50$ and 100 MeV respectively.

- Tangential pressure:** Tangential pressure (p_t) actually maintains the spherical shape of the compact star by counteracting the outward radial pressure (p_r). Depending on various factors, such as specific stellar composition, EoS etc., the behaviour of p_t can vary. However, the nature of radial and tangential pressure profiles are similar, i.e., consistently decreasing from the stellar core to boundary and it is demonstrated in figures 9 and 10 for the three phases within the parameter space used here. Notably, p_t is also positive at all internal points of the configuration, which points towards a physically acceptable stellar structure. Here, figures 9, 10a and 10b describe the radial variation of tangential pressure p_t profiles across the three phases. Moreover, we note that with increasing strange quark mass (m_s) the magnitude of p_t increases within the choice of parameter space.

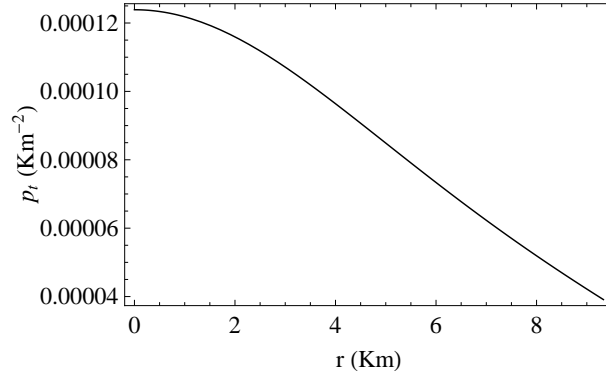


Figure 9: Radial variation of tangential pressure (p_t) for $2SC$ phase.

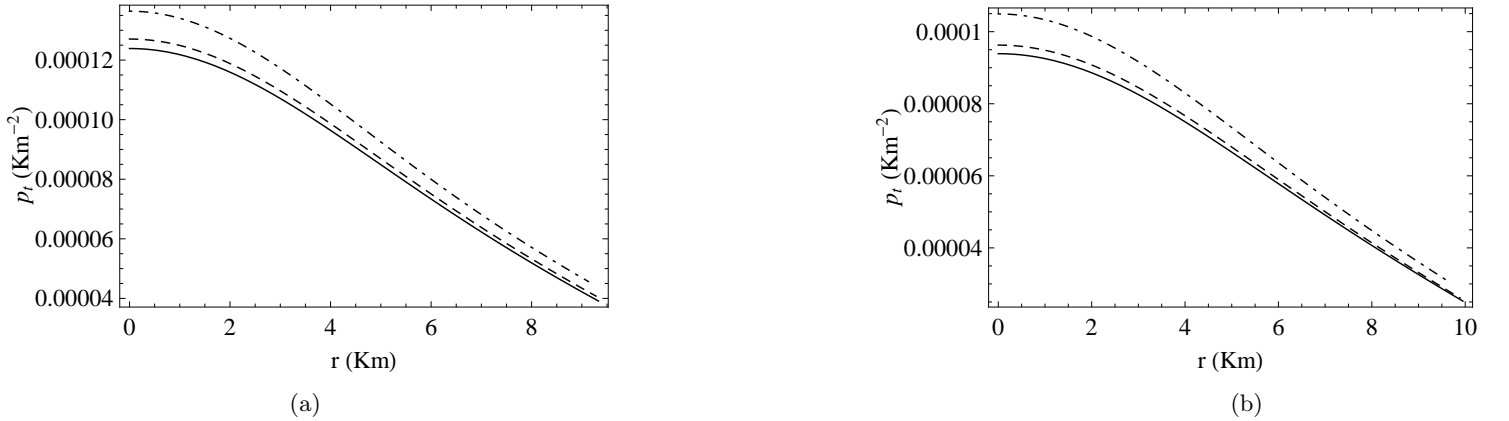


Figure 10: Radial variation of tangential pressure (p_t) for (a) $2SC + s$ phase and (b) CFL phase. Here, the solid, dashed and dotdashed lines represent $m_s = 0, 50$ and 100 MeV respectively.

- Pressure anisotropy:** The anisotropy in pressure (Δ_a) is the difference between the radial and tangential pressures, i.e., $\Delta_a = p_t - p_r$. Figures 11, 12a and 12b illustrate the radial variation of pressure anisotropy for the three phases respectively. Additionally, we note that $\Delta_a > 0$ in all the phases, which depict a repulsive anisotropic behaviour. Notably, from figure 12, it is observed that with increasing strange quark mass (m_s), Δ_a increases within this parameter space. This feature can be attributed to several reasons, *viz.*, (i) strange quarks (s) are heavier than u and d quarks. Now, increasing the mass of s quarks leads to a mass disparity which ultimately alters the momentum distribution and the interaction among quarks. This imbalance can lead to an uneven distribution of forces, contributing to anisotropy in the pressure, (ii) larger m_s softens the EoS. As a result the effective pressures in different directions become more sensitive to mass difference, which amplifies the anisotropic behaviour, (iii) The interaction between quarks in the dense matter is influenced by their masses. An increase in strange quark mass strengthens the role of strong interactions and modifies the confinement properties which may lead to differential pressure contributions in different directions, thereby enhancing the pressure anisotropy.

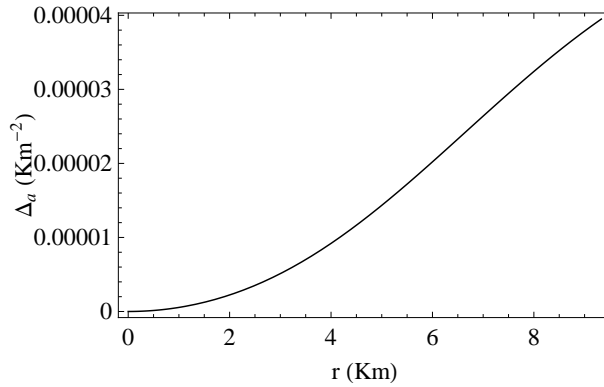


Figure 11: Radial variation of pressure anisotropy (Δ_a) for 2SC phase.

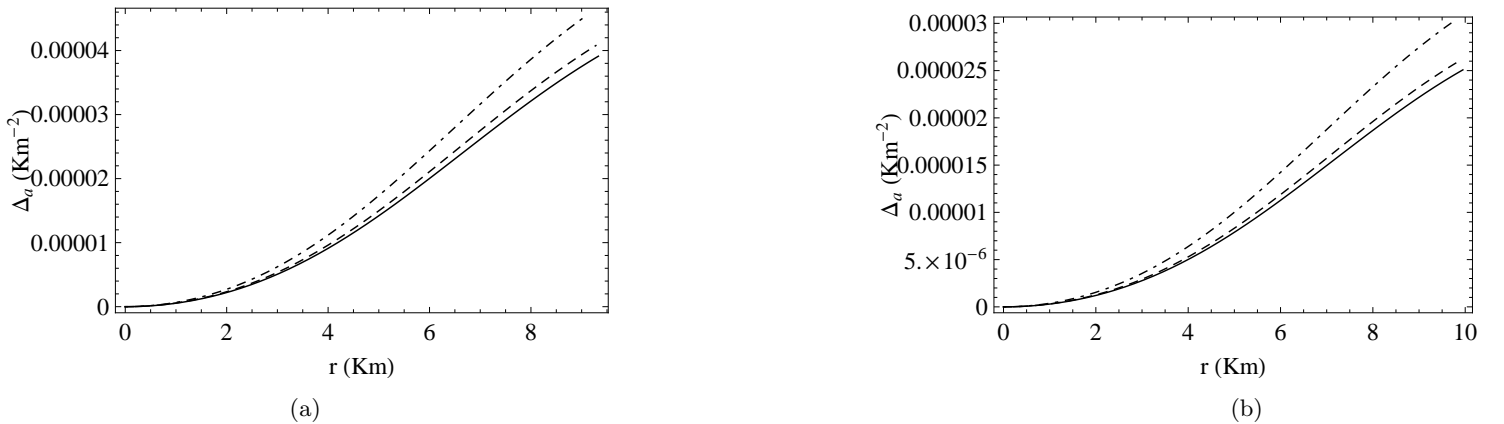


Figure 12: Radial variation of pressure anisotropy (Δ_a) for (a) 2SC + s phase and (b) CFL phase. Here, the solid, dashed and dotdashed lines represent $m_s = 0, 50$ and 100 MeV respectively.

8.2 Causality condition

To develop a realistic model for an anisotropic compact star, a crucial aspect is the analysis of sound wave propagation within its dense interior. The radial and tangential sound velocities are defined as $v_r^2 = \frac{dp_r}{d\rho}$ and $v_t^2 = \frac{dp_t}{d\rho}$, respectively, where ρ , p_r and p_t have been previously introduced. Adopting natural units ($\hbar = c = 1$), the causality condition enforces an upper limit on the sound velocities, requiring $v_r^2 \leq 1$ and $v_t^2 \leq 1$. Additionally, thermodynamic stability demands that $v_r^2 > 0$ and $v_t^2 > 0$. Consequently, the sound velocities must satisfy the combined constraints $0 < v_r^2 \leq 1$ and $0 < v_t^2 \leq 1$ throughout the stellar interior. Notably, following the IQM EoS as expressed in eq. (8), we note that the radial sound velocity, $v_r^2 = \frac{dp_r}{d\rho} = \frac{1}{3}$, throughout all the phases, however, the tangential sound velocity (v_t^2) varies with strange quark mass (m_s). To address the complexity of these relationships, we have chosen to illustrate the radial variation of the tangential sound velocities graphically, as shown in figures 13 and 14. Figure 13 is subjected to the 2SC phase whereas figures 14a and 14b denote the 2SC + s and CFL phases respectively. Evidently, the causality conditions are consistently upheld throughout the stellar interior within the chosen parameter space.

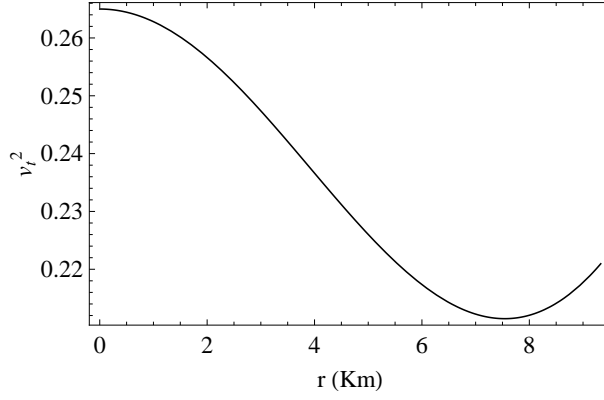


Figure 13: Radial variation of tangential sound velocity (v_t^2) for $2SC$ phase.

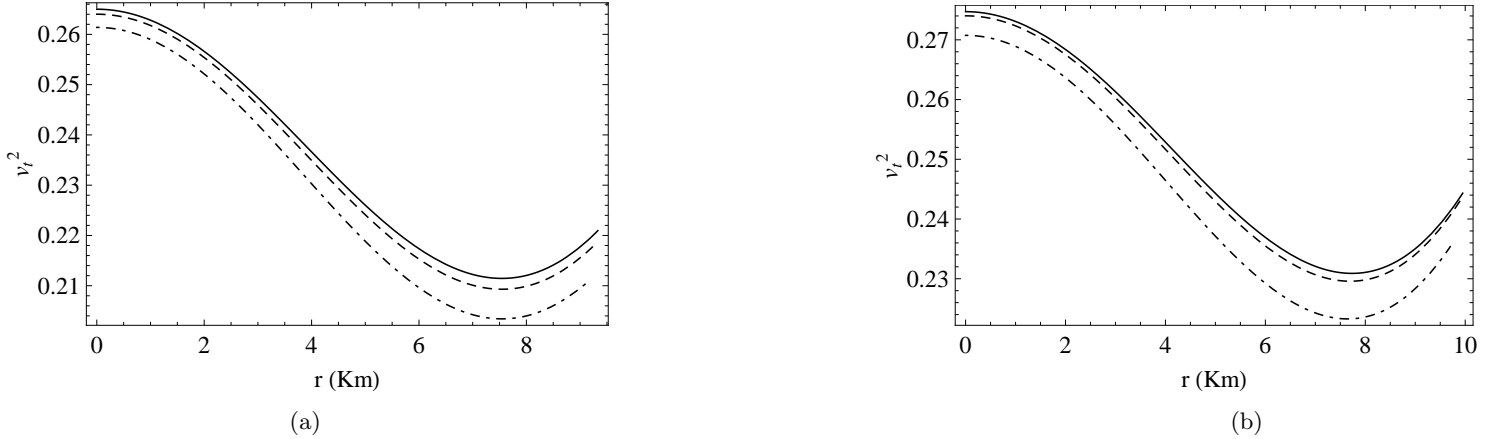


Figure 14: Radial variation of tangential sound velocity (v_t^2) for (a) $2SC + s$ phase and (b) CFL phase. Here, the solid, dashed and dotdashed lines represent $m_s = 0, 50$ and 100 MeV respectively.

8.3 Energy conditions

In gravitational theory, energy conditions impose constraints on matter distributions, serving as essential guidelines for formulating a physically valid energy-momentum tensor. These conditions offer a framework for analysing the properties of matter distributions without requiring detailed knowledge of the internal composition. Consequently, phenomena such as the formation of geometric singularities or gravitational collapse during mergers can be studied without explicitly specifying the pressure or energy density. Fundamentally, the analysis of energy conditions is an algebraic problem [102], specifically an eigenvalue problem associated with the energy-momentum tensor. In a 4-dimensional space-time, evaluating these conditions involves solving a quartic polynomial to determine its eigenvalues, which can become analytically intricate. Despite the challenges in obtaining general solutions, a physically viable fluid distribution must satisfy the dominant, strong, weak, and null energy conditions, collectively referred to as the energy conditions [102, 103, 104], within the stellar configuration. In this work, following the presence of IQM EoS, we assess these energy conditions for the present stellar model using the formulations provided in [105, 106] as:

- NEC: $T_{ij}l^i l^j \geq 0 \Rightarrow \rho + p_r \geq 0, \rho + p_t \geq 0,$
- WEC: $T_{ij}t^i t^j \geq 0 \Rightarrow \rho \geq 0, \rho + p_r \geq 0, \rho + p_t \geq 0,$
- SEC: $T_{ij}t^i t^j - \frac{1}{2}T_k^k t^\sigma t_\sigma \geq 0 \Rightarrow \rho + \sum p \geq 0, \text{ or, } \rho + p_r \geq 0, \rho + p_t \geq 0, \rho + p_r + 2p_t \geq 0,$
- DEC: $T_{ij}t^i t^j \geq 0 \Rightarrow \rho \geq 0, \rho - p_r \geq 0, \rho - p_t \geq 0,$

where, l^i and t^i are time-like and null vectors respectively. Figures 15 and 16 indicate that the necessary energy conditions are adequately satisfied within the parameter space utilised in the present model.

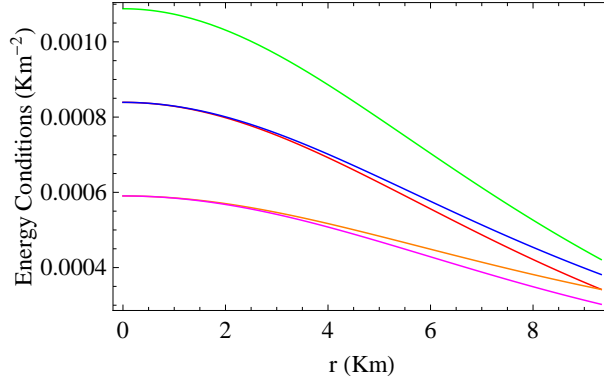


Figure 15: Radial variation of energy conditions for 2SC phase. Here, Red, Blue, Green, Orange and Magenta lines represent $(\rho + p_r)$, $(\rho + p_t)$, $(\rho + p_r + 2p_t)$, $(\rho - p_r)$ and $(\rho - p_t)$ respectively.

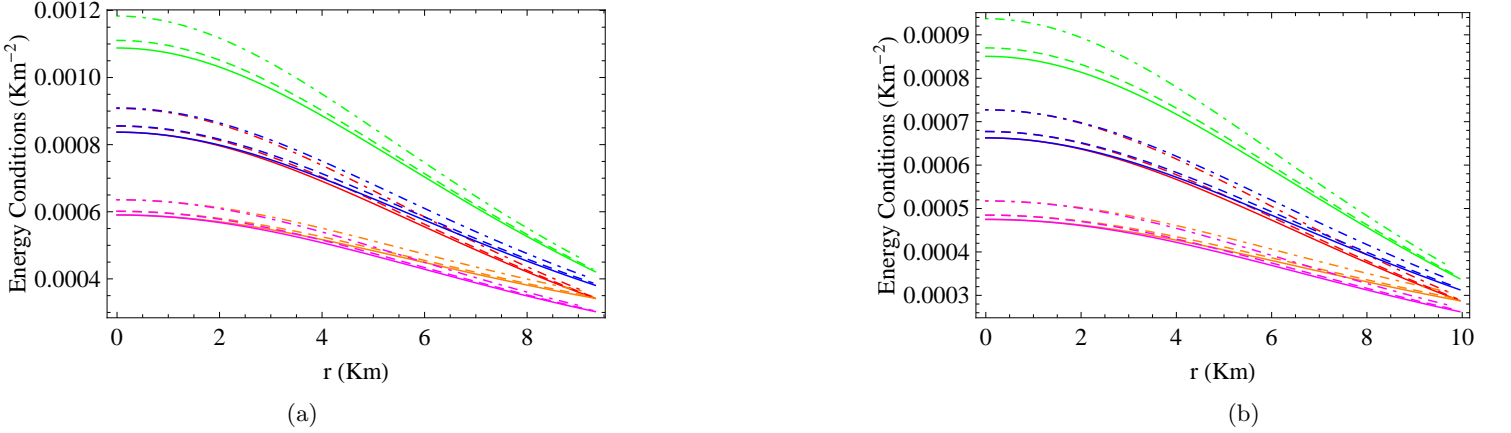


Figure 16: Radial variation of energy conditions for (a) 2SC + s phase and (b) CFL phase. Here, Red, Blue, Green, Orange and Magenta lines represent $(\rho + p_r)$, $(\rho + p_t)$, $(\rho + p_r + 2p_t)$, $(\rho - p_r)$ and $(\rho - p_t)$ respectively. Moreover, the solid, dashed and dotdashed lines represent $m_s = 0, 50$ and 100 MeV respectively.

9 Stability analysis

The stability of the proposed model is addressed through the following methods:

- TOV equation in a generalised form,
- Herrera cracking condition, and,
- Adiabatic index

9.1 TOV equation in a generalised form

The physical viability of a stellar model, in terms of hydrostatic equilibrium, can be assessed through stability analysis, which examines the interplay of various forces within the stellar configuration. For a compact star with pressure anisotropy, this analysis considers three key force components: (i) the gravitational force (F_g), (ii) the hydrostatic force (F_h), and, (iii) the anisotropic force (F_a). To achieve stable equilibrium, these forces must collectively balance each other. In this work, we evaluate stability using the generalised form of the Tolman-Oppenheimer-Volkoff (TOV) equation [92, 93], as presented below:

$$-\frac{M_G(\rho + p_r)}{r^2}e^{\lambda-\nu} - \frac{dp_r}{dr} + \frac{2\Delta_a}{r} = 0. \quad (53)$$

The active gravitational mass, represented as M_G and defined in Eq. (53), can be obtained from the mass formula proposed by Tolman-Whittaker [107], expressed in the following form:

$$M_G(r) = r^2\nu'e^{\nu-\lambda}. \quad (54)$$

Substituting Eq. (54) into Eq. (53), we obtain:

$$-\nu'(\rho + p_r) - \frac{dp_r}{dr} + \frac{2\Delta_a}{r} = 0. \quad (55)$$

Using the demarcation as written below:

$$F_g = -\nu'(\rho + p_r), \quad (56)$$

$$F_h = -\frac{dp_r}{dr}, \quad (57)$$

$$F_a = \frac{2\Delta_a}{r}, \quad (58)$$

we rewrite eq. (55) in the form:

$$F_g + F_h + F_a = 0. \quad (59)$$

By substituting eqs. (33), (34), (35) and (36), in eq. (59), the equilibrium condition outlined in the generalised TOV equations is derived. To simplify the presentation and circumvent mathematical intricacies, the stable equilibrium condition is illustrated graphically. Figures 17 and 18 illustrate that our mode is in stable equilibrium under the impact of difference

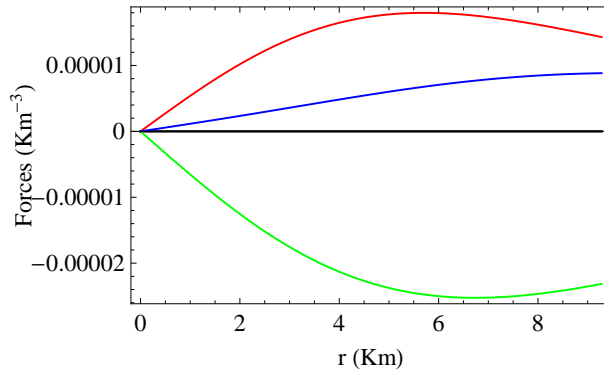


Figure 17: Radial variation of different forces for 2SC phase. Here, Green, Red and Blue lines represent F_g , F_h and F_a respectively.

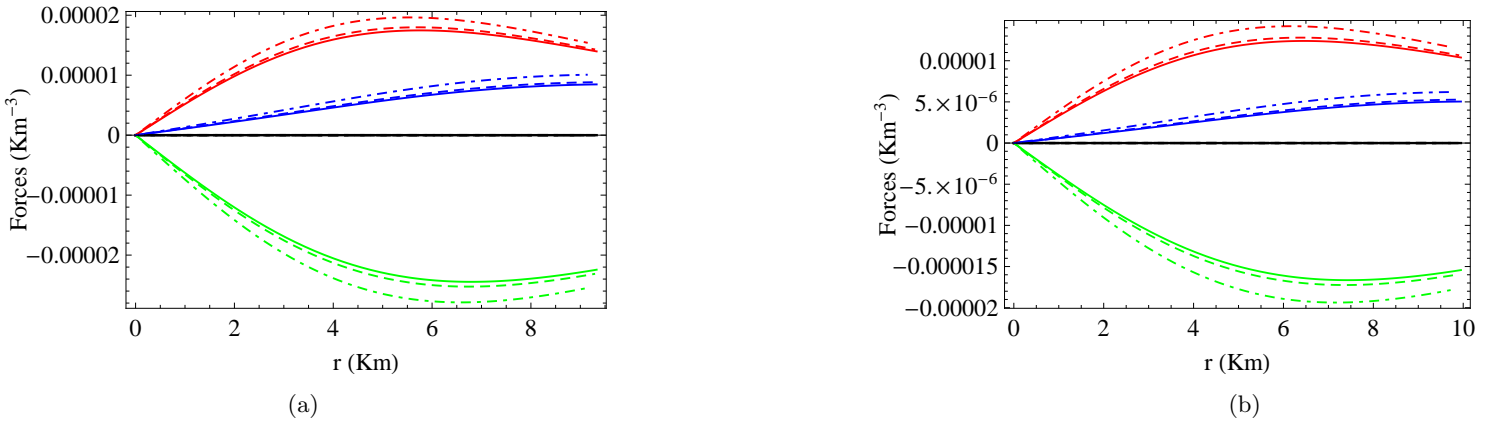


Figure 18: Radial variation of different forces for (a) 2SC + s phase and (b) CFL phase. Here, Green, Red and Blue lines represent F_g , F_h and F_a respectively. Moreover, the solid, dashed and dotted lines represent $m_s = 0, 50$ and 100 MeV respectively.

forces, across the three phases within this parameter space.

9.2 Herrera cracking condition

Herrera [108] introduced the concept of "Cracking" in the context of a fluid sphere within a self-gravitating compact object. This term refers to the total radial forces of opposing signs that emerge when the system experiences perturbations. When considering the EoS, cracking can occur under two conditions: (i) in the presence of a locally anisotropic fluid or (ii) in a

slowly contracting and radiating perfect fluid. Using this framework, Abreu et al. [109] investigated how local anisotropy influences the distribution of an anisotropic fluid. They showed that when perturbations are present, the potential stability of the system can be determined by the difference between the squares of the radial (v_r^2) and tangential (v_t^2) sound velocities, as expressed in the following relation:

$$0 \leq |v_t^2 - v_r^2| \leq 1. \quad (60)$$

A stellar model satisfying this relation is considered a stable structure. From figures 19, 20a and 20b, it is evident that the Abreu inequality is consistently upheld throughout the stellar interior for the $2SC$, $2SC + s$ and CFL phases respectively within the chosen parameter space.

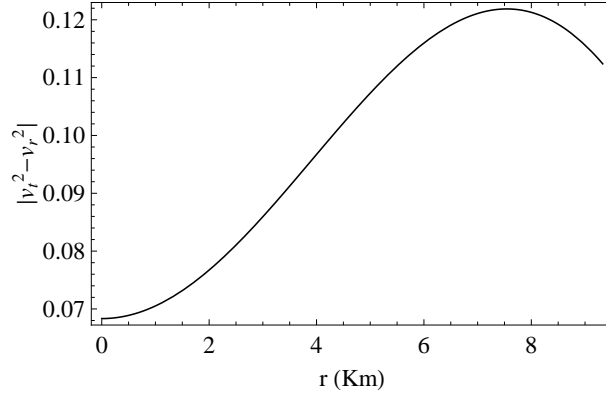


Figure 19: Radial variation of $|v_t^2 - v_r^2|$ for $2SC$ phase.

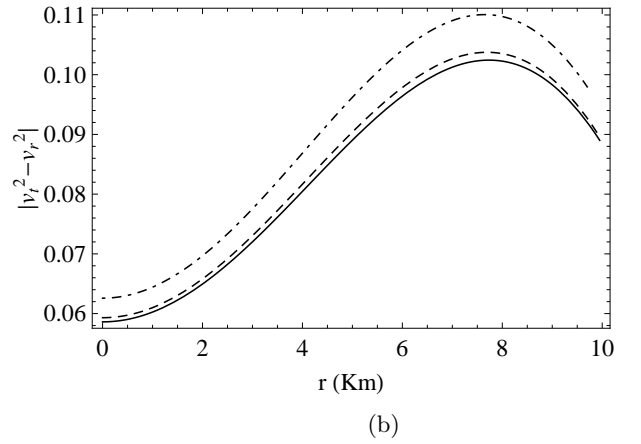
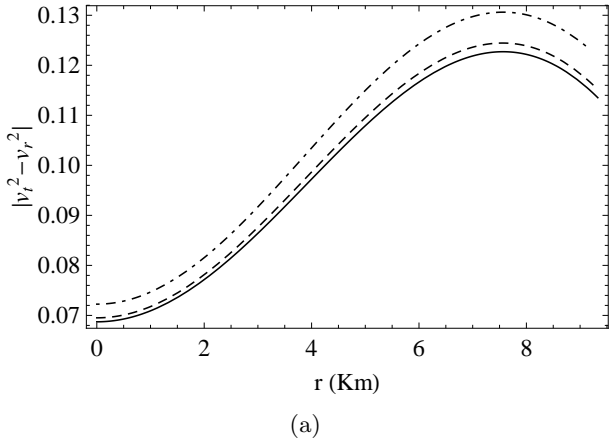


Figure 20: Radial variation of $|v_t^2 - v_r^2|$ for (a) $2SC + s$ phase and (b) CFL phase. Here, the solid, dashed and dot-dashed lines represent $m_s = 0, 50$ and 100 MeV respectively.

9.3 Adiabatic index

The adiabatic index (Γ) indicates the stiffness of the EoS at a given density. In the framework of a relativistic anisotropic stellar structure, the adiabatic index is expressed as:

$$\Gamma = \frac{\rho + p_r}{p_r} \frac{dp_r}{dr} = \frac{\rho + p_r}{p_r} v_r^2. \quad (61)$$

Heintzmann and Hillebrandt [74] showed that for a Newtonian matter distribution, the adiabatic index satisfies $\Gamma > \frac{4}{3}$. Subsequently, Chan et al. [110] extended this upper bound for the adiabatic index by taking pressure anisotropy into account, as expressed in the following form:

$$\Gamma > \Gamma', \quad (62)$$

where,

$$\Gamma' = \frac{4}{3} - \left[\frac{4(p_r - p_t)}{3|p_r'|r} \right]_{max}. \quad (63)$$

Now, to determine the anisotropic limit as expressed in eq. (63), we have evaluated Γ' for different values of strange quark mass (m_s) for the three phases. The results are graphically represented in figures 21, 22a and 22b. Based on figures 21

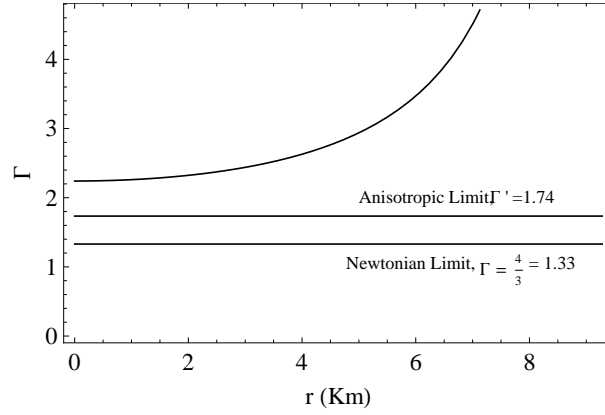
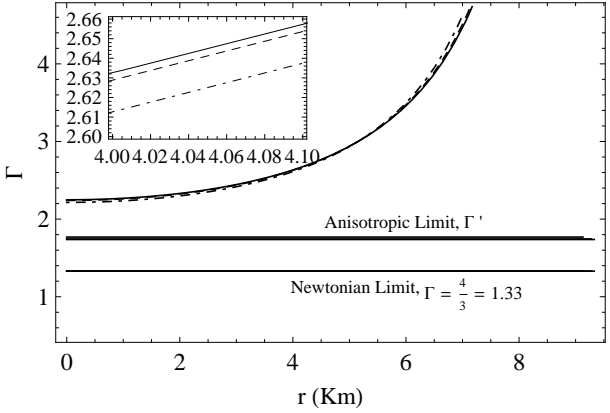
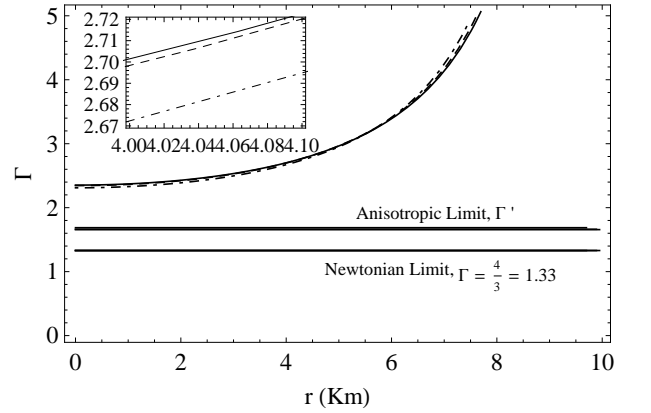


Figure 21: Radial variation of adiabatic index for 2SC phase.



(a)



(b)

Figure 22: Radial variation of adiabatic index for (a) 2SC + s phase and (b) CFL phase. Here, the solid, dashed and dotdashed lines represent $m_s = 0, 50$ and 100 MeV respectively.

and 22, we may assert that the current model preserves the notion of the radial variation of adiabatic index, as required for a stable anisotropic stellar model, to emerge as a physically acceptable stellar structure across the three phases, within the parameter space utilised here.

10 Discussion

The MIT bag model, despite its simplicity, has long been the preferred framework for studying quark matter in compact stars. Fundamental questions, such as the potential presence of deconfined matter in NS cores, have traditionally been explored while disregarding interactions among the system's constituents. Within the Standard Model of particle physics, QCD is recognised as the fundamental theory governing the strong interactions between quarks mediated by gluons. Given the QCD framework, it is evident that existing weak-coupling EoS for cold quark matter require refinement to provide a more realistic depiction of quark matter cores in compact stars.

This study adheres to a simple yet parameterised EoS for cold quark matter that addresses the limitations of the bag model and other low-energy effective models by incorporating the properties of IQM. Leveraging perturbative QCD expansions and colour superconductivity, we provide a framework that accounts for inter-quark effects arising from strong interactions, which may uncover novel physical phenomena under extreme conditions of matter and gravity subjected to the interior of compact stars. Specifically, we explore the impact of strong interactions on anisotropic quark stars composed of IQM within the symmetric teleparallel $f(Q)$ theory of gravity. By considering a spherically symmetric space-time, we employ the Buchdahl-I metric ansatz [86] and IQM EoS, as expressed in eq. (8), alongside a linear form of the $f(Q)$ action which enables the construction of singularity-free and regular solutions of the EFE under the $f(Q)$ theory of gravity.

Based on the work of Zhang and Mann [26], it is observed that the numerical values of the constant coefficients in the EoS give rise to three distinct phases of quark matter within the configuration, *viz.*, (i) the pairing of u and d quarks (udQM) is termed the $2SC$ phase, (ii) the inclusion of s quarks in udQM leads to $2SC + s$ phase and (iii) CFL phase. To examine these physical acceptability of the present model in these phases, we have chosen the LMXB 4U 1608-52 [100] as a representative candidate and analysed its properties across the three phases. Our findings, presented both numerically and graphically, focus on the effects of varying the strange quark mass (m_s) for the $2SC$, $2SC + s$ and CFL phases respectively. Key characteristic features of the configuration have been identified and analysed in detail below:

- We begin by imposing the restrictions on the particular choices of strange quark mass (m_s), colour superconductivity (Δ) and bag constant (B_g), through the evaluation of energy per baryon (\mathcal{E}_B) for the three phases. Figures 1 and 2 illustrates the variation of \mathcal{E}_B vs. Δ for the three phases respectively. The energy per baryon (\mathcal{E}_B) of the most stable nuclei, *i.e.*, ${}^{56}Fe$ is $930.4 MeV$. Hence, to describe a stable quark matter, \mathcal{E}_B has to be less than $930.4 MeV$. Figures 1 and 2 demonstrate the variation of \mathcal{E}_B for $B_g = 70 MeV/fm^3$ and different choices of strange quark mass, $m_s = 0, 50$ and $100 MeV$. Following figures 1 and 2, we note that the notion of $\mathcal{E}_B < 930.4 MeV$ is well preserved in this formalism. Therefore, the numerical choices of $\Delta = 100 MeV$, $B_g = 70 MeV/fm^3$ and $m_s = 0, 50$ and $100 MeV$ are justified in the present model. Moreover, from figure 1, it is evident that udQM possesses a lower energy per baryon relative to SQM which further supports its stability. Moreover, with increasing m_s , we note that \mathcal{E}_B increases for the $2SC + s$ and CFL phases as shown in figures 2a and 2b respectively.
- To determine the maximum mass and the corresponding radius in this interacting quark system, we have numerically solved the TOV equations within the parametric choices of microscopic parameters for the three phases. Figures. 3 and 4 graphically illustrate the concerned results for the $2SC$, $2SC + s$ and CFL phases respectively. Further, from figures 4a and 4b we note that in the $2SC + s$ and CFL phases, the maximum mass decreases with increasing strange quark mass (m_s), which denotes a softening of the EoS. This may be attributed to the fact that, with increasing m_s , the energy density increases which may accelerate the gravitational collapse of the structure thereby reducing the maximum mass and the associated radius. The maximum mass and radius for all the three phases are tabulated in table 1. As evident from figures 3 and 4 and table 1, the mass-radius comparison indicates that the CFL phase supports a more massive stellar structure than other phases [94]. Moreover, in table 2, we have predicted the radii of some compact star candidates for the three phases and different values of m_s . Additionally, tables 3 and 4 describe the central density (ρ_0), surface density (ρ_s) and central pressure (p_0) across the three phases, within the parameter space used here.
- The radial variation of the thermodynamic parameters such as energy density (ρ), radial (p_r) and tangential (p_t) pressures are demonstrated in figures 5, 6, 7, 8, 9 and 10, throughout the three phases. We note that in all the phases ($2SC$, $2SC + s$ and CFL), the physical characteristic parameters maintain a monotonically decreasing nature. In particular, for the $2SC + s$ and CFL phases, the energy density and pressure profiles increase with increasing value of m_s . In figures 11 and 12, the pressure anisotropy profiles are shown. Additionally, the anisotropy is positive in all the three phases, with depicts a repulsive anisotropic nature. In the context of $2SC + s$ and CFL phases, we have observed that the magnitude of anisotropy increases with increasing value of m_s . Several factors contribute to this phenomenon: (i) the heavier mass of strange quarks (s) compared to u and d quarks introduces mass disparities, affecting momentum distribution and pressure anisotropy, (ii) increased m_s softens the EoS, amplifying directional pressure sensitivity, and (iii) stronger interactions from higher m_s modify confinement, enhancing anisotropy.
- Within the parameter space used here, the causality and the necessary energy conditions are well maintained throughout the stellar boundary.

- Within this IQM system and $f(Q)$ formalism, the stability of the present model is addressed through several well acknowledged methodologies, *viz.*, the generalised TOV equations, Herrera's concept of cracking and the radial variation of adiabatic index. Figures 17 and 18 demonstrate that the present model is in hydrostatic equilibrium under the influence of different forces across the three phases. The stability criteria based on the concept of cracking and Abreu inequality [109] is well maintain in this model as evident from figures 19 and 20. Further, from figures 21 and 22, we have noted that the adiabatic index variation for an anisotropic stellar model is well supported in the present formalism.

In conclusion, we may assert that the $f(Q)$ gravity framework proves effective in developing physically consistent stellar models compatible with fundamental principles in static, spherically symmetric space-times. By incorporating an IQM EoS that captures strong quark interactions at high densities, this formalism provides a realistic depiction of stellar matter under extreme conditions. Thus, the proposed model represents a stable and physically viable description to explore the structural and dynamical properties of quark stars, composed of interacting quark matter, within the $f(Q)$ gravity framework.

11 Acknowledgments

DB is thankful to the Department of Science and Technology (DST), Govt. of India, for providing the fellowship vide no: DST/INSPIRE Fellowship/2021/IF210761. DB and KBG are thankful to the Department of Physics, Cooch Behar Panchanan Barma University for providing the necessary help to carry out the research work. PKC gratefully acknowledges support from IUCAA, Pune, India under Visiting Associateship programme.

References

- [1] C. M. Will, *The Confrontation between General Relativity and Experiment*, *Living Rev. Relativ.* **17** (2014) 4 [arXiv:1403.7377].
- [2] G. Baym et al., *From hadrons to quarks in neutron stars: a review*, *Rep. Prog. Phys.* **81** (2018) 056902 [arXiv:1707.04966v3].
- [3] M. Feroci et al., *The Large Observatory for X-ray Timing (LOFT)*, *Exp. Astron.* **34** (2012) 415 [arXiv:1107.0436].
- [4] P. de Forcrand, *Simulating QCD at finite density*, *PoS LAT2009* (2009) 010 [arXiv:1005.0539].
- [5] J. M. Lattimer, *The Nuclear Equation of State and Neutron Star Masses*, *Annu. Rev. Nucl. Sci.* **62** (2012) 485 [arXiv:1305.3510].
- [6] E. Farhi and R. L. Jaffe, *Strange matter*, *Phys. Rev. D* **30** (1984) 2379.
- [7] N. Itoh, *Hydrostatic Equilibrium of Hypothetical Quark Stars*, *Prog. Theor. Phys.* **44** (1970) 291.
- [8] J. Madsen, *Physics and astrophysics of strange quark matter*, in *Hadrons in Dense Matter and Hadrosynthesis, Lecture Notes in Physics*, vol 516, ed. by J. Cleymans, H. B. Geyer, F. G. Scholtz (Heidelberg: Springer, 1998), p. 42 [astro-ph/9809032].
- [9] G. Baym and S.A. Chin, *Can a neutron star be a giant MIT bag?*, *Phys. Lett. B* **62** (1976) 241.
- [10] C. Alcock, E. Farhi and A. Olinto, *Strange Stars*, *Astrophys. J.* **310** (1986) 261.
- [11] N.K. Glendenning, *FAST PULSARS, STRANGE STARS: AN OPPORTUNITY IN RADIO ASTRONOMY*, *Mod. Phys. Lett. A* **05** (1990) 2197.
- [12] E. Witten, *Cosmic separation of phases*, *Phys. Rev. D* **30** (1984) 272.
- [13] B. Holdom, J. Ren and C. Zhang, *Quark Matter May Not Be Strange*, *Phys. Rev. Lett.* **120** (2018) 222001 [arXiv:1707.06610].
- [14] C. Zhang, *Probing up-down quark matter via gravitational waves*, *Phys. Rev. D* **101** (2020) 043003 [arXiv:1908.10355].
- [15] Q. Wang, C. Shi and H. S. Zong, *Nonstrange quark stars from an NJL model with proper-time regularization*, *Phys. Rev. D* **100** (2019) 123003 [arXiv:1908.06558].

- [16] T. Zhao et al., *Do the current astronomical observations exclude the existence of non-strange quark stars?*, *Phys. Rev. D* **100** (2019) 043018 [arXiv:1904.09744].
- [17] C. J. Xia et al., *Supercritically charged objects and electron-positron pair creation*, *Phys. Rev. D* **101** (2020) 103031 [arXiv:2001.03531].
- [18] B. Acharya et al. (MoEDAL Collaboration), *First Search for Dyons with the Full MoEDAL Trapping Detector in 13 TeV pp Collisions*, *Phys. Rev. Lett.* **126** (2021) 071801 [arXiv:2002.00861].
- [19] L. W. Piotrowski et al., *Limits on the flux of nuclearites and other heavy compact objects from the "Pi of the Sky" project*, *Phys. Rev. Lett.* **125** (2020) 091101 [arXiv:2008.01285].
- [20] E. P. Zhou, X. Zhou and A. Li, *Constraints on interquark interaction parameters with GW170817 in a binary strange star scenario*, *Phys. Rev. D* **97** (2018) 083015 [arXiv:1711.04312].
- [21] G. F. Burgio et al., *Are small radii of compact stars ruled out by GW170817/AT2017gfo?*, *Astrophys. J.* **860** (2018) 139 [arXiv:1803.09696].
- [22] Z. Roupas, G. Panotopoulos and I. Lopes, *QCD color superconductivity in compact stars: color-flavor locked quark star candidate for the gravitational-wave signal GW190814*, *Phys. Rev. D* **103** (2021) 083015 [arXiv:2010.11020].
- [23] J. E. Horvath and P. H. R. S. Moraes, *Modelling a 2.5 M_{\odot} Compact Star with Quark Matter*, *Int. J. Mod. Phys. D* **30** (2021) 2150016 [arXiv:2012.00917].
- [24] T. Harko, K. S. Cheng and Z. Kovacs, *Can stellar mass black holes be quark stars?*, *Mon. Not. Roy. Astron. Soc.* **400** (2009) 1632 [arXiv:0908.2672].
- [25] J. Ren and C. Zhang, *Quantum nucleation of up-down quark matter and astrophysical implications*, *Phys. Rev. D* **102** (2020) 083003 [arXiv:2006.09604].
- [26] C. Zhang and R. B. Mann, *Unified Interacting Quark Matter and its Astrophysical Implications*, *Phys. Rev. D* **103** (2011) 063018 [arXiv:2009.07182].
- [27] Z. Cao et al., *GW190814: Circumstantial Evidence for Up-Down Quark Star*, *Phys. Rev. D* **106** (2022) 083007 [arXiv:2009.00942].
- [28] E. S. Fraga, R.D. Pisarski, and J. Schaffner-Bielich, *Small, dense quark stars from perturbative QCD*, *Phys. Rev. D* **63** (2001) 121702 [arXiv:hep-ph/0101143].
- [29] E. S. Fraga, A. Kurkela and A. Vuorinen, *Interacting quark matter equation of state for compact stars*, *Astrophys. J. Lett.* **781** (2014) L25 [arXiv:1311.5154].
- [30] M.G. Alford, K. Rajagopal, and F. Wilczek, *Color-Flavor Locking and Chiral Symmetry Breaking in High Density QCD*, *Nucl. Phys. B* **537** (1999) 443 [arXiv:hep-ph/9804403].
- [31] K. Rajagopal and F. Wilczek, *Enforced Electrical Neutrality of the Color-Flavor Locked Phase*, *Phys. Rev. Lett.* **86** (2001) 3492 [arXiv:hep-ph/0012039].
- [32] G. Lugones and J.E. Horvath, *Color-flavor locked strange matter*, *Phys. Rev. D* **66** (2002) 074017 [arXiv:hep-ph/0211070].
- [33] R. Abbott et al. (LIGO Scientific and Virgo Collaborations), *GW190814: Gravitational Waves from the Coalescence of a 23 Solar Mass Black Hole with a 2.6 Solar Mass Compact Object*, *Astrophys. J. Lett.* **896** (2020) L44 [arXiv:2006.12611].
- [34] J. M. Z. Pretel et al., *Effects of anisotropic pressure on interacting quark star structure*, *Phys. Lett. B* **848** (2024) 138375 [arXiv:2311.18770v2].
- [35] A. Errehymy et al., *Study of anisotropic quark stars with interacting quark matter in $f(R, T)$ gravity*, *J. High Energy Astrophys.* **44** (2024) 410.
- [36] T. Tangphati et al., *Interacting quark star with pressure anisotropy and recent astrophysical observations*, *Chin. J. Phys.* **91** (2024) 392.
- [37] H. Weyl, *Eine neue Erweiterung der Relativitätstheorie.*, *Ann. der Phys.* **364** (1919) 101.
- [38] A. Einstein, *Sitzber. Preuss. Akad. Wiss.* **17** (1928) 217.

- [39] K. Hayashi and T. Shirafuji, *New general relativity*, *Phys. Rev. D* **19** (1979) 3524.
- [40] T. Sauer, *Field equations in teleparallel spacetime: Einstein's Fernparallelismus approach towards unified field theory*, *Historia Mathematica* **33** (2006) 399 [arXiv:physics/0405142v1].
- [41] J. M. Nester, H.-J. Yo, *Symmetric teleparallel general relativity*, *Chin. J. Phys.* **37** (1999) 113 [arXiv:gr-qc/9809049].
- [42] J. B. Jiménez, L. Heisenberg and T. Koivisto, *Coincident General Relativity*, *Phys. Rev. D* **98** (2018) 044048 [arXiv:1710.03116v2].
- [43] L. Heisenberg, *A systematic approach to generalisations of General Relativity and their cosmological implications*, *Phys. Rep.* **796** (2019) 1 [arXiv:1807.01725v1].
- [44] M. Hohmann et al., *Propagation of gravitational waves in symmetric teleparallel gravity theories*, *Phys. Rev. D* **99** (2019) 024009 [arXiv:1808.02894v3].
- [45] I. Soudi et al., *Polarization of gravitational waves in symmetric teleparallel theories of gravity and their modifications*, *Phys. Rev. D* **100** (2019) 044008.
- [46] R. Lazkoz et al., *Observational constraints of $f(Q)$ gravity*, *Phys. Rev. D* **100** (2019) 104027 [arXiv:1907.13219v2].
- [47] F. D' Ambrosio et al., *Black holes in $f(Q)$ gravity*, *Phys. Rev. D* **105** (2022) 024042.
- [48] M. Calzá and L. Sebastiani, *Eur. Phys. J. C* **83** (2023) 3 247.
- [49] F. Bajardi, D. Vernieri and S. Capozziello, *Bouncing Cosmology in $f(Q)$ Symmetric Teleparallel Gravity*, *Eur. Phys. J. Plus* **135** (2020) 912 [arXiv:2011.01248v1].
- [50] W. Khylllep, A. Paliathanasis and J. Dutta, *Cosmological solutions and growth index of matter perturbations in $f(Q)$ gravity*, *Phys. Rev. D* **103** (2021) 103521 [arXiv:2103.08372v2].
- [51] I. Ayuso, R. Lazkoz and V. Salzano, *Observational constraints on cosmological solutions of $f(Q)$ theories*, *Phys. Rev. D* **103** (2021) 063505 [arXiv:2012.00046v1].
- [52] L. Heisenberg, *Review on $f(Q)$ Gravity*, *Phys. Rep.* **1066** (2024) 1 [arXiv:2309.15958v1].
- [53] B. J. Barros et al., *Testing $f(Q)$ gravity with redshift space distortions*, *Phys. Dark Universe* **30** (2020) 100616.
- [54] J. B. Jiménez et al., *Cosmology in $f(Q)$ geometry*, *Phys. Rev. D* **101** (2020) 103507.
- [55] F. K. Anagnostopoulos, S. Basilakos and E. N. Saridakis, *First evidence that non-metricity $f(Q)$ gravity could challenge Λ CDM*, *Phys. Lett. B* **822** (2021) 136634 [arXiv:2104.15123v2].
- [56] K. Flathmann and M. Hohmann, *Post-Newtonian limit of generalized symmetric teleparallel gravity*, *Phys. Rev. D* **103** (2021) 044030 [arXiv:2012.12875v1].
- [57] F. D'Ambrosio, L. Heisenberg and S. Zentarra, *Hamiltonian Analysis of $f(Q)$ Gravity and the Failure of the Dirac-Bergmann Algorithm for Teleparallel Theories of Gravity*, [arXiv:2308.02250v1].
- [58] M. Adeel et al., *Physical analysis of anisotropic compact stars in $f(Q)$ gravity*, *Mod. Phys. Lett. A* **38** (2023) 2350152 .
- [59] S.K. Maurya et al., *The Effect of Gravitational Decoupling on Constraining the Mass and Radius for the Secondary Component of GW190814 and Other Self-bound Strange Stars in $f(Q)$ Gravity Theory*, *Astrophys. J. Suppl. Ser.* **269** (2023) 35 [arXiv:2309.10130].
- [60] A. Errehymy et al., *Anisotropic electrically charged stars in $f(Q)$ symmetric teleparallel gravity*, *Eur. Phys. J. Plus* **137** (2022) 1311.
- [61] S. V. Lohakare et al., *Influence of three parameters on maximum mass and stability of strange star under linear $f(Q)$ -action*, *Mon. Not. R. Astron. Soc.* **526** (2023) 3796 [arXiv:2309.10830v1].
- [62] P. Bhar, A. Malik and A. Almas, *Impact of $f(Q)$ gravity on anisotropic compact star model and stability analysis*, *Chin. J. Phys.* **88** (2024) 839.
- [63] P. Bhar and J. M. Z. Pretel, *Dark energy stars and quark stars within the context of $f(Q)$ gravity*, *Phys. Dark Universe* **42** (2023) 101322.

- [64] P. Bhar, *Existence of Dark Energy Stars within Lower Mass Gap in the Realm of $f(Q)$ Gravity*, *Fortschritte der Physik* **71** (2023) 2300074.
- [65] M. Z. Gul et al., *Viable and stable compact stars in $f(Q)$ theory*, *Eur. Phys. J. C* **84** (2024) 8 [arXiv:2401.08692].
- [66] R. Ruderman, *PULSARS: STRUCTURE AND DYNAMICS*, *Astron. Astrophys.* **10** (1972) 427.
- [67] V. Canuto, *EQUATION OF STATE AT ULTRAHIGH DENSITIES*, *Ann. Rev. Astron. Astrophys.* **12** (1974) 167.
- [68] R. Kippenhahn and A. Weigert, *Stellar Structure and Evolution* (Springer, Berlin, 1990).
- [69] R.A. Broglia and V. Zelevinsky (eds.), *Fifty Years of Nuclear BCS: Pairing in Finite Systems* (World Scientific Publishing Co. Pte. Ltd., Singapore, 2013).
- [70] R. F. Sawyer and D. J. Scalapino, *Pion Condensation in Superdense Nuclear Matter*, *Phys. Rev. D* **8** (1973) 1260.
- [71] R. F. Sawyer, *Condensed π^- Phase in Neutron-Star Matter*, *Phys. Rev. Lett.* **29** (1972) 382.
- [72] L. Herrera and N. O. Santos, *Local anisotropy in self-gravitating systems*, *Phys. Rep.* **286** (1997) 53.
- [73] R.L. Bowers and E. P. T. Liang, *ANISOTROPIC SPHERES IN GENERAL RELATIVITY*, *Astrophys. J.* **188** (1974) 657.
- [74] H. Heintzmann and W. Hillebrandt, *Neutron Stars with an Anisotropic Equation of State: Mass, Redshift and Stability*, *Astron. Astrophys.* **38** (1975) 51.
- [75] B. Carter and D. Langlois, *Relativistic models for Superconducting-Superfluid Mixtures*, *Nucl. Phys. B* **531** (1998) 478 [arXiv:gr-qc/9806024v1].
- [76] S.K. Maurya et al., *Anisotropic models for compact stars*, *Eur. Phys. J. C* **75** (2015) 225 [arXiv:1504.00209v2].
- [77] S.K. Maurya et al., *Relativistic anisotropic models for compact star with equation of state $p = f(\rho)$* , *Int. J. Mod. Phys. D* **26** (2017) 1750002.
- [78] D. Deb et al., *Relativistic model for anisotropic strange stars*, *Ann. Phys. (N. Y.)* **387** (2017) 239 [arXiv:1606.00713v2].
- [79] M. K. Mak and T. Harko, *Anisotropic Stars in General Relativity*, *Proc. Roy. Soc. Lond. A* **459** (2003) 393.
- [80] M. K. Mak et al., *EXACT MODELS FOR ANISOTROPIC RELATIVISTIC STARS*, *Int. J. Mod. Phys. D* **11** (2002) 207.
- [81] H. Hernandez and L. Nunez, *Nonlocal Equation of State in Anisotropic Static Fluid Spheres in General Relativity*, *Can. J. Phys.* **82** (2004) 29.
- [82] D. Bhattacharjee and P. K. Chattopadhyay, *Maximum mass of an anisotropic compact object admitting the modified Chaplygin equation of state in Buchdahl-I metric*, *Eur. Phys. J. C* **84** (2024) 77 [arXiv:2310.07391v1].
- [83] M. Alford and K. Rajagopal, *Absence of two-flavor color-superconductivity in compact stars*, *J. High Energy Phys.* **0206** (2002) 031 [hep-ph/0204001].
- [84] M. Alford et al., *Hybrid stars that masquerade as neutron stars*, *Astrophys. J.* **629** (2005) 969 [arXiv:nucl-th/0411016].
- [85] S. Weissenborn et al., *Quark Matter In Massive Compact Stars*, *Astrophys. J. Lett.* **740** (2011) L14 [arXiv:1102.2869].
- [86] H. A. Buchdahl, *General Relativistic Fluid Spheres*, *Phys. Rev.* **116** (1959) 1027.
- [87] W. Wang, H. Chen and T. Katsuragawa, *Static and spherically symmetric solutions in $f(Q)$ gravity*, *Phys. Rev. D* **105** (2022) 024060 [arXiv:2110.13565v2].
- [88] C. G. Böhrer, A. Mussa and N. Tamanini, *Existence of relativistic stars in $f(T)$ gravity*, *Class. Quantum Gravity* **28** (2011) 245020.
- [89] K. Schwarzschild, *On the Gravitational Field of a Mass Point according to Einstein's Theory*, *Sitzungsber. Preuss. Akad. Wiss. Berlin (Math. Phys.)* **1916** (1916) 189.

- [90] J. L. Rosa, *Junction conditions in gravity theories with extra scalar degrees of freedom*, *Phys. Rev. D* **109** (2024) 064018 [arXiv:2311.11752].
- [91] J. L. Rosa, N. Ganiyeva and F.N.S. Lobo, *Non-exotic traversable wormholes in $f(R, T_{ab}^{ab})$ gravity*, *Eur. Phys. J. C* **83** (2023) 1040.
- [92] R. C. Tolman, *Static Solutions of Einstein's Field Equations for Spheres of Fluid*, *Phys. Rev.* **55** (1939) 364.
- [93] J. R. Oppenheimer and G. M. Volkoff, *On Massive Neutron Cores*, *Phys. Rev.* **55** (1939) 374.
- [94] K. B. Goswami, A. Saha, P. K. Chattopadhyay and S. Karmakar, *A new mass limit ($3.61M_{\odot}$) of strange star admitting CFL equation of state*, *Eur. Phys. J. C* **83** (2023) 1038 [arXiv:2304.01629v1].
- [95] F. Özel, T. Güver and D. Psaltis, *THE MASS AND RADIUS OF THE NEUTRON STAR IN EXO 1745-248*, *Astrophys. J.* **693** (2009) 1775.
- [96] T. Güver et al., *THE MASS AND RADIUS OF THE NEUTRON STAR IN 4U 1820-30*, *Astrophys. J.* **719** (2010) 1807 [arXiv:1002.3825].
- [97] M. L. Rawls et al., *Refined Neutron Star Mass Determinations for Six Eclipsing X-Ray Pulsar Binaries*, *Astrophys. J.* **730** (2011) 25 [astro-ph.SR/1101.2465].
- [98] M. K. Abubekеров et al., *The mass of the compact object in the X-ray binary her X-1/HZ her*, *Astron.Rep.* **52** (2008) 379 [astro-ph.SR/1201.5519].
- [99] P. C. C. Freire et al., *On the nature and evolution of the unique binary pulsar J1903+0327*, *Mon. Not. R. Astron. Soc* **412** (2010) 2763 [arXiv:1011.5809].
- [100] T. Güver et al., *THE DISTANCE, MASS, AND RADIUS OF THE NEUTRON STAR IN 4U 1608-52*, *Astrophys. J.* **712** (2010) 964 [arXiv:0811.3979v4].
- [101] S. K. Maurya et al., *The Effect of Gravitational Decoupling on Constraining the Mass and Radius for the Secondary Component of GW190814 and Other Self-bound Strange Stars in $f(Q)$ Gravity Theory*, *Astrophys. J. Suppl. Ser.* **269** (2023) 35.
- [102] C. A. Kolassis, N. O. Santos and D. Tsoubelis, *Energy conditions for an imperfect fluid*, *Class. Quantum Gravity* **5** (1988) 1329.
- [103] S. W. Hawking and G. F. R. Ellis, *The Large Scale Structure of Spacetime* (Cambridge University Press: Cambridge, UK), (1973).
- [104] R. Wald, *General Relativity* (University of Chicago Press: Chicago, IL, USA), (1984).
- [105] B. P. Brassel, S. D. Maharaj and R. Goswami, *Inhomogeneous and Radiating Composite Fluids*, *Entropy* **23** (2021) 1400.
- [106] B. P. Brassel, S. D. Maharaj and R. Goswami, *Higher-dimensional inhomogeneous composite fluids: energy conditions*, *Prog. Theor. Exp. Phys.* **2021**, 103E01 (2021) (20 pages).
- [107] Ø Grøn, *Repulsive gravitation and electron models*, *Phys. Rev. D* **31** (1985) 2129.
- [108] L. Herrera, *Cracking of self-gravitating compact objects*, *Phys. Lett. A* **165** (1992) 206.
- [109] H. Abreu, H. Hernandez and L. A. Núñez, *Sound speeds, cracking and the stability of self-gravitating anisotropic compact objects* *Class. Quantum Gravity* **24** (2007) 4631 [arXiv:0706.3452v2].
- [110] R. Chan, L. Herrera and N.O. Santos, *Dynamical instability for radiating anisotropic collapse*, *Mon. Not. R. Astron. Soc.* **265** (1993) 533.